

# Resonant Solitary States in Complex Networks

Jakob Niehues,<sup>1,2,3</sup> Serhiy Yanchuk,<sup>1,2,4</sup> Rico Berner,<sup>2</sup> Jürgen Kurths,<sup>1,2</sup> Frank Hellmann,<sup>1</sup> and Mehrnaz Anvari<sup>1,5</sup>

<sup>1</sup>*Potsdam Institute for Climate Impact Research (PIK),*

*Member of the Leibniz Association, P.O. Box 60 12 03, D-14412 Potsdam, Germany*

<sup>2</sup>*Humboldt-Universität zu Berlin, Department of Physics, Newtonstraße 15, 12489 Berlin, Germany*

<sup>3</sup>*Technische Universität Berlin, ER 3-2, Hardenbergstrasse 36a, 10623 Berlin, Germany*

<sup>4</sup>*University College Cork, School of Mathematical Sciences, Western Road, Cork, T12 XF62, Ireland*

<sup>5</sup>*Fraunhofer Institute for Algorithms and Scientific Computing, 53757 Sankt Augustin, Germany*

Partially synchronized solitary states occur frequently when a synchronous system of networked oscillators is perturbed locally. Remarkably, several asymptotic states of different frequencies can coexist at the same node. Here, we uncover the mechanism underlying this multistability: The resonant back-reaction of the network's modes on the solitary can lead to a large energy transfer between them, and the solitary's frequency adaptation can tune the system to this resonance. We provide a full analytic analysis of this mechanism, and show which network structures enable its presence.

Oscillator systems are ubiquitous in the description of natural and human-made systems. Important extended systems as diverse as the heart, the brain, firefly populations, chemical reactions, and power grids, can be modelled as networks of interconnected oscillators [1–5]. One of the most fundamental common aspects of the collective behavior of such systems is synchronization [6]. In some, such as the power grid, it is essential for their proper functioning, in others, such as the brain, it can indicate severe dysfunction. The tendency to synchronize, and thus the function of the system, is strongly influenced by the underlying network's topology.

The paradigmatic models for understanding this relationship between structure and function in coupled oscillator networks are the Kuramoto model [7] and its variants. These feature extremely rich collective behavior, such as chimera states, frequency clusters, isolated desynchronization, and spatial chaos [1–5]. The Kuramoto model with inertia [8, 9] has been developed independently to study synchronization properties in power grids [10, 11] and biological systems [12].

The transition from decoupling to synchrony in inertial Kuramoto networks is characterized by spatial chaos, a form of extreme multistability [13]. This regime typically has several states with similarly sized basins of attraction [14, 15]. Among the most prominent are frequency clusters [16, 17], the simplest of which are solitary states. In a solitary state, only one or a few oscillators start to rotate at their own frequencies, while the rest of the network remains synchronized [18, 19]. Solitary states are especially prominent for the important situation of localized large perturbations [20–22], and they are particularly likely for perturbations at leaf nodes [20, 23]. Localized perturbations are important in systems like power grids, where single component failures are common and can lead to desynchronization and blackouts [24].

Interestingly, numerical studies have revealed that solitary nodes can exist not only at the natural frequency of the oscillators, but also at shifted frequencies in networks

with losses [21] and at intermediate frequencies [23]. In addition, the presence of multistability in these solitary nodes has been identified, allowing for the coexistence of both intermediate and natural solitary states [15, 23] at the same node.

Previous work has discussed the role of a networks' topology in understanding its overall response to perturbations and the emergence of various stable states [5, 20, 23, 25, 26]. In some contexts, the frequency and stability of the solitary states have been studied in terms of decoupling and entrainment arguments [21, 27]. These explanations do not account for either intermediate frequency solitaires or the coexistence of several solitary states at the same node. In the following, we use averaging theory [28] and linear response to develop a theory of the resonant coupling between the synchronized cluster and the solitary. We uncover that the described phenomena arise from the cluster's resonantly excited complex network structure. This leads to a non-zero mean energy flow between cluster and solitary, and a frequency shift (Fig. 1). While works like [29–31] have previously considered the interaction between individual oscillators and the mean field, such an interaction between collective network modes and individual oscillators has not been previously described.

In the following, we will use the Kuramoto model with inertia. This is given by the coupled second-order equations

$$m_i \ddot{\varphi}_i = P_i - \alpha_i \dot{\varphi}_i - \sum_{j=1}^N p_{ij}(\varphi_i, \varphi_j), \quad (1)$$

where  $\varphi_i$  are the phases of the  $N$  oscillators,  $P_i$  the driving powers, the  $m_i$  are inertia constants, and the  $\alpha_i > 0$  are damping coefficients. The coupling is given in terms of the weighted coupling matrix  $\{\kappa_{ij}\}$  as  $p_{ij}(\varphi_i, \varphi_j) = \kappa_{ij} \sin(\varphi_i - \varphi_j)$ .

In a synchronous state,  $\varphi_i^*, \dot{\varphi}_i^* = \hat{\omega}$ , the phases satisfy  $P_i - \alpha_i \hat{\omega} = \sum_{j=1}^N p_{ij}(\varphi_i^*, \varphi_j^*)$ . By going to a corotat-

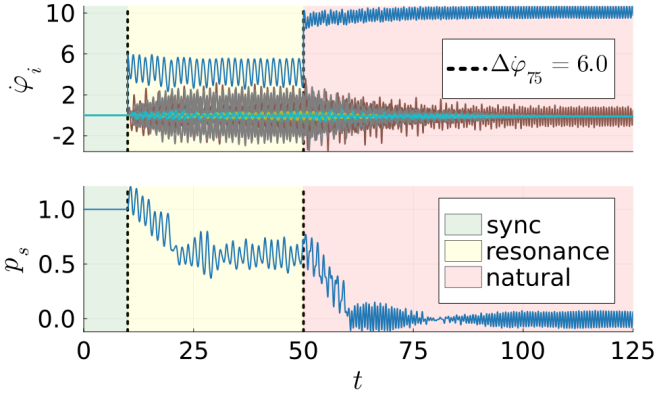


FIG. 1. Frequencies ( $\varphi_i$ ) and time-averaged energy flow  $p_s$  between solitary and synchronous component for a complex oscillator network following two single-node frequency perturbations, see supplementary material (SM) for an animation and the network topology (Fig. S2) [32]. The first perturbation brings the system from the synchronized regime into an intermediate solitary state in resonance with the synchronized cluster. The second perturbation causes the transition to a natural solitary state, where the solitary node is effectively decoupled and the oscillations of the synchronized cluster are much smaller. The distinct blue trajectory belongs to the solitary node 75 in Fig. 2.

ing frame, we can always set  $\hat{\omega} = 0$ , and will assume so from now on. The  $p_{ij}(\varphi_i^*, \varphi_j^*)$  can be interpreted as the energy flowing through the network to balance out the driving powers  $P_i$ , (this is the physical interpretation for power grids), and  $\alpha_i$  determines the restoring force of the frequency. The natural frequencies of the uncoupled oscillators (i.e., when all  $\kappa_{ij} = 0$ ) are determined by the condition that driving power and restoring force balance:  $\Omega_i := P_i/\alpha_i$ .

Figure 2 shows the asymptotic frequencies actually observed following single node perturbations in a complex network generated with [33] for which  $\Omega_i = \pm 10$ . When perturbations occur at nodes 74, 75 and 84, they induce intermediate frequencies. These nodes are leaves with a highly connected neighbor. Further, intermediate frequencies occur for all such nodes in this network.

*Ansatz and averaging.*— We will begin by introducing an ansatz for describing a solitary leaf node  $z$  and a synchronized cluster  $S = \{i : 1 \leq i \leq N, i \neq z\}$ . For simplicity, we will assume that  $\alpha_i$  and  $m_i$  are constant throughout  $S$ . Node  $z$  is connected to  $S$  through the intermediary node  $k \in S$ . The coupling between them is given by  $p_{zk}$ , which we decompose into a long-term time average  $p_s = \langle p_{zk} \rangle$  and a mean zero part:  $p_{zk}(t) := p_s + p_{zk}^{\text{osc}}(t)$ . Our ansatz is

$$\varphi_i(t) = \omega_{\text{sync}} t + \vartheta_i^* + \vartheta_i(t) \quad \text{for } i \in S, \quad (2)$$

$$\varphi_z(t) = \omega_s t + \vartheta_k^* + \vartheta_z(t). \quad (3)$$

Here, we define  $\omega_{\text{sync}}$  and  $\omega_s$  as the long term average frequency of the synchronized cluster, and the solitary

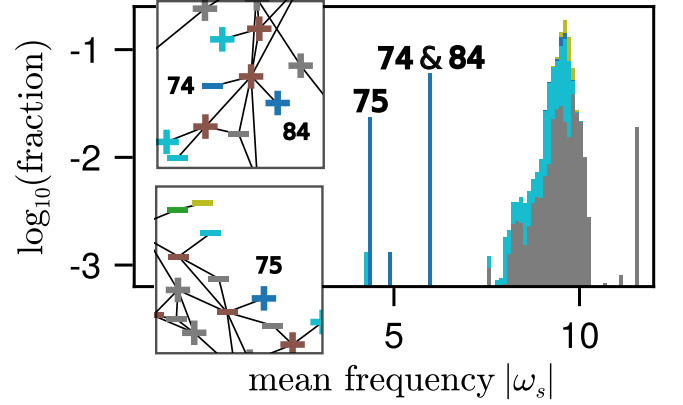


FIG. 2. Asymptotic solitary frequencies in a synthetic power grid after perturbations. Three solitary states are clearly distinct from the natural frequencies at  $\pm 10$ . They occur at leaf nodes with highly connected neighbors (cf. [23]) nodes 74, 75 and 84, shown in the insets. Nodes shown as '+' ('-') have  $P_i = 1$  ( $-1$ ). States are counted as desynchronized if there are frequencies whose absolute value exceeds the threshold  $\omega_{th} = 1$ , and as solitary if there is exactly one desynchronized node, cf. Fig. S4. Shown here is the absolute value of  $\omega_s$ , which coincides with  $\omega_s \cdot \text{sgn}(P_i)$  for each node  $i$ . See Fig. S2 for the full network, and Fig. 1 for a solitary state of node 75.

oscillator, respectively. The  $\vartheta_i^*$  are a synchronous state of  $S$  given a fixed power injection  $p_s$  at  $k$ .

Solitary states are those for which  $\vartheta_i(t)$  and  $\vartheta_z(t)$  are bounded and the corotating solitary frequency, defined as  $\omega_c := \omega_s - \omega_{\text{sync}}$ , is non-zero. It can also be shown by summing over Eq. (1), that  $(N-1)\alpha\omega_{\text{sync}} + \alpha_z\omega_s = 0$ . This gives us

$$\omega_c(\omega_s) = \left(1 + \frac{\alpha_z}{(N-1)\alpha}\right) \omega_s. \quad (4)$$

Now, a central step is to linearize the equations around  $\vartheta_i = 0$ . This is justified numerically, as the synchronized oscillators remain relatively close to the synchronous state. To linear order in  $\vartheta_k$ ,  $p_{zk}$  is

$$p_{zk}(t) = \kappa_{zk} \{ \sin[\omega_c t + \vartheta_z(t)] - \vartheta_k(t) \cos[\omega_c t + \vartheta_z(t)] \}. \quad (5)$$

Introducing the vectors  $e_i^k := \delta_{ik}$ , and  $\vec{\vartheta}$  with components  $\vartheta_i$  for all  $i \in S$ , the system is

$$m\ddot{\vec{\vartheta}} = -\alpha\dot{\vec{\vartheta}} - L^*\vec{\vartheta} + e^k p_{zk}^{\text{osc}}(t), \quad (6)$$

$$m_z\ddot{\vartheta}_z = P_z - \alpha_z(\dot{\vartheta}_z + \omega_s) - p_s - p_{zk}^{\text{osc}}(t), \quad (7)$$

where  $L^*$  is the effective coupling Laplacian on the synchronized cluster with weights  $\kappa_{ij} \cos(\vartheta_i^* - \vartheta_j^*)$ .

Note that  $p_s$  does not appear in the equation for  $S$ , since the synchronized cluster steady state accounts for the average power injection from the solitary. We also

note that the dependence of  $L^*$  on  $p_s$  is typically weak (SM I.B).

For  $\vartheta_z$  to stay bounded, and for  $\omega_s$  to be the long-term average of the solitary's frequency, the long-term average  $\vartheta_z$  has to be zero. This provides us with the condition  $0 = P_z - \alpha_z \omega_s - p_s$ .  $p_s$  is a measure for the mean coupling of  $S$  and  $z$ , while  $\omega_s$  stands for their incoherence. Note that this relationship between  $\omega_s$  and  $p_s$  can be observed in Fig. 1. In synchrony there is a steady high energy flow. In the natural solitary state, the mean energy flow is zero and the system is effectively decoupled. For intermediate solitary states, there is some intermediate amount of energy.

If we now can express  $p_s$  as a function of  $\omega_s$ , this equation becomes a self-consistent equation for the frequency of the solitary state:

$$0 = Z(\omega_s) := P_z - \alpha_z \omega_s - p_s(\omega_s). \quad (8)$$

Additionally, a potentially stable solitary state requires the correct sign of the change in  $Z$  with frequency. If we imagine  $\omega_s$  as slowly varying, we have  $m_z \dot{\omega}_s = Z(\omega_s)$ . Thus, we expect the sign of the derivative  $\partial_{\omega_s} Z(\omega_s)$  to be informative about the stability of the solitary state, at least heuristically.

Both  $p_s$  and  $\omega_s$  depend on the trajectory of the solution. To obtain the relationship between them, we will leverage averaging theorems [28] to obtain an approximate solution for which they can be exactly evaluated. To do so, we introduce a timescale  $\varepsilon^{-1}$  that splits the slow, non-rotating and the rotating dynamics. By rescaling the time axis we can eliminate  $m$  in Eq. (1), and set  $\alpha$ ,  $P$ , and  $\kappa$  to  $\varepsilon$ ,  $\varepsilon P$  and  $\varepsilon \kappa$  for a small value  $\varepsilon$ . We choose  $\varepsilon$  such that while the rescaled  $\kappa$  remains of order one, the eigenvalues of the rescaled effective Laplacian  $L^*$  for the eigenmodes localized at  $k$  are of order  $\varepsilon^{-1}$ . As a result, we treat  $L^r = \varepsilon L^*$  as being of order one. Such a scaling can be achieved, if node  $k$  has a sufficiently high degree (SM I.A).

After this rescaling, Eq. (6) and Eq. (7) become

$$\ddot{\vec{\vartheta}} = \varepsilon \left[ -\dot{\vec{\vartheta}} + e^k p_{zk}^{\text{osc}}(t) \right] - L^r \vec{\vartheta}, \quad (9)$$

$$\ddot{\vartheta}_z = \frac{\varepsilon m}{m_z} \left[ P_z - \frac{\alpha_z}{\alpha} \dot{\vartheta}_z - p_{zk}(t) \right]. \quad (10)$$

Equation (9) has the form of the perturbation of the Hamiltonian system  $\ddot{\vec{\vartheta}} = -L^r \vec{\vartheta}$ , where the perturbation is due to  $\vartheta_z$ . The appropriate perturbative approach in this case is averaging [28], where one should first write the system for the slowly varying amplitudes of the network modes, i.e., the amplitudes of the periodic solutions of the unperturbed system, see Eq. (S48). The amplitude dynamics is then decomposed into modes resonant with  $\omega_c$ , the driving frequency in  $p_{zk}^{\text{osc}}$ , and non-resonant ones. The contributions of both types of modes are small, allowing us to average the dynamics of  $\vec{\vartheta}$ . We obtain  $\vartheta_k(t)$

and insert it into Eq. (10). We then average Eq. (10) and undo the rescaling in this equation to obtain the explicit form of the self-consistent Eq. (8):

$$Z(\omega_s) = P_z - \alpha_z \omega_s - \frac{\kappa_{zk}^2}{2} \sum_{\ell=1}^{N-1} \frac{\alpha \omega_c \left( v_k^{[\ell]} \right)^2}{\left( \lambda^{[\ell]} - m \omega_c^2 \right)^2 + \alpha^2 \omega_c^2}. \quad (11)$$

In Eq. (11), the sum runs over eigenmodes  $\ell$  of  $L^*$ , with eigenvalue  $\lambda^{[\ell]}$  and eigenvector  $v^{[\ell]}$ . To efficiently evaluate Eq. (11), we assume that the dependence of  $L^*$  and its eigenmodes on  $p_s$  is weak. This is a reasonable assumption if the synchronized cluster is significantly larger than the solitary cluster (node  $k$ ) and the energy injected at node  $k$  dissipates quickly into  $S$ .

*A linear response picture.*— The obtained form of  $p_s$  has a natural interpretation. The solitary state, with frequency  $\omega_c$ , perturbs the synchronized cluster. The response of the cluster has the frequency  $\omega_c$  and some well-defined phase shift. This enables a non-zero energy flow  $p_s$  between  $S$  and  $z$ , which is responsible for the frequency shift  $\omega_s$ . The flow is proportional to the amplitude of the response and the local amplitude of the corresponding eigenvector. Thus, large energy flows can occur if  $\omega_c$  is close to resonance with an eigenmode of  $S$  that is localized at  $k$ . As  $\omega_c$  shifts with the energy flow, the system can robustly tune itself towards such resonances if they are present. This resonant tuning mechanism predicts why certain topological features, namely the ones causing highly localized modes, enable the generation of additional solitary states.

Following this interpretation, we can directly derive the result for  $Z(\omega_s)$  in Eq. (11) using linear response theory, if we neglect the nonlinear part of  $p_{zk}^{\text{osc}}$  in Eq. (9), which is eventually averaged out in the averaging approach, from the outset. This alternative assumption can be justified, when this nonlinearity is only one of several contributions to the overall coupling of a well-connected node  $k$ . In this case, the network is harmonically driven by  $\sin \omega_c t$ , and linear response similar to [26] can be used to calculate its response, including the amplitudes  $a_k^{(k)[\ell]}(\omega_c)$  and phase lags  $\delta^{[\ell]}(\omega_c)$  at the driven node  $k$ . These then provide us with a time averaged energy flow:

$$p_s(\omega_c) = -\frac{\kappa_{kz}}{2} \sum_{\ell=1}^N a_k^{(k)[\ell]}(\omega_c) \sin \delta^{[\ell]}(\omega_c). \quad (12)$$

Both approaches used to derive Eq. (11) straightforwardly generalize to a solitary node connected to several nodes in  $S$ . The back-reactions of the network combine linearly, and we simply sum over all neighbors of  $z$  (Eq. (S71)).

*Examples.*— We illustrate the power of Equation (11) using two examples. First we give a minimal effective model that exhibits the resonant tuning mechanism

cleanly; then a full complex network with a complex resonant response. We compare the results with numerical simulations [34]. Further examples can be found in the SM II.B.

The simplest model that shows tristability with two distinct solitary frequencies is a system that neglects the response of the network beyond the node  $k$ . We have a solitary node ( $z = 1$ ), its neighbor ( $k = 2$ ), and the rest of the network is assumed to have infinite inertia, and thus no dynamics. This model is shown in the inset in Fig. 3 (right). The neighbor has  $n$  links into the infinitely heavy part, each with coupling strength  $K$ . See SM II.A for details.

The left panel in Fig. 3 shows the energy absorbed by frequency adaptation, a straight line given by  $P_1 - \alpha\omega_s$ , and the energy flow due to the network's response,  $p_s = \langle p_{12} \rangle$ . There is a single peak centered around the only network mode, which is close to  $\lambda = \sqrt{Kn}$ . At the intersection of these two curves, we have a zero of Eq. (11). However, the linear stability heuristic suggests that only intersections with  $\partial_{\omega_s} Z < 0$  are candidates for stable solitary states. Graphically, these correspond to intersections where the network response intersects from below when reading left to right.

Hence, for  $n \lesssim 12$ , there is a pair of a stable and an unstable solution due to the peak, and a third, stable solution at  $\omega_s \approx \Omega_1 = P_1/\alpha$ . For larger values of  $n$ , the second and third solutions annihilate, while the first converges to  $\omega_s = \Omega_1$ . The bifurcation diagram in the right panel of Fig. 3 illustrates this behavior. Numerical simulations with random initial conditions closely correspond to the predicted frequency and stability of solitary states, confirming the existence of tristability between the synchronous state and solitary states at multiple frequencies, and the overall accuracy of our results.

We now apply our result to the complex network shown in Figs. 2 and S2. Solitary states with intermediate frequency are located at leaves with neighbor degree  $\geq 6$ , (cf. [23]). Figure 4 shows the solutions of Eq. (11) for  $z = 74$  for slightly heterogeneous parameters.

As many network modes are excited, the response curve is considerably more complex. However, simulation results reveal that there is still one dominant mode with high localization at the root node  $k$ , which is in close resonance with the solitary frequency, and which occurs frequently from random initial conditions.

There are several tentative observations we can make by looking at these examples, (Figs. S4 and S5): (i) Eq. (11) tends to underestimate the magnitude of the most prominent solution for  $\omega_s$  slightly, this can already be observed in the effective model; (ii) pairs of close stable and unstable solutions, which are caused by narrow peaks, result in solitary states with a small basin of attraction; (iii) pairs close to their annihilating bifurcation, caused by peaks that barely exceed the straight line at the intersection, also cause small basins; (iv) the most

prominent solitary state lies at a frequency that has a high and broad peak and some distance to the next solutions.

Leaf nodes with high neighbor degree [23], typically produce category (iv) situations (SM I.A). Thus, these findings explain why such nodes feature solitary states with intermediate frequencies.

The derivation of the minimal model, and the explicit relationship between network mode and neighbor degree (SM I.A and II.A), suggests that the neighbor degree can serve as an upper bound of the intermediate frequency in the complex network case. This is also observed numerically (Fig. S8).

*Conclusion.*— We present an analytical description of the effective coupling between a solitary oscillator and the synchronized cluster in a complex network. To approximate the trajectories, we utilize partial linearization and an averaging theorem. This way, we discover that a resonant excitation of the linear modes of the synchronized cluster can couple coherently to the shifted frequency of the solitary state, resulting in a large energy flow between the synchronized cluster and the solitary oscillator and effectively shifting the frequency.

Our framework predicts the location of solitary oscillations in reduced models, and is in excellent agreement with what we see in complex networks. With this, we can explain that solitary states appear mostly in specific parts of the network [16], more specifically leaves and tree-shaped structures, which act as weak points in perturbation scenarios [15, 20, 23, 35]. These results have important implications for improving grid stability through modifications of parameters [36–38], topology [20, 39–41], and targeted control [42].

While the presented mechanism can explain the potential existence and stability of intermediate solitary states, there are still open questions that require further investigation. A key practical question is the estimation of the basin boundaries of these states, which would provide deeper insights into the dynamics and robustness of synchronous systems, against perturbations [15, 31, 35, 43, 44].

Detailed numerical studies suggest that additional classes of attractive states exist, and the interaction of losses on the lines and resonant energy flow remains unexplored [21]. Furthermore, a more detailed study of the interaction of multiple solitary nodes with distinct frequencies or in frequency clusters is needed.

Finally, while the method introduced above focuses on phase oscillators, it would be interesting to extend it to phase-amplitude oscillators that play a central role in networks such as power grids [45]. We expect that the overall analytical approach we introduced can be further developed and adapted to address these types of questions.

The code for reproducing our simulations and figures can be found in [46]. The repository can also be applied

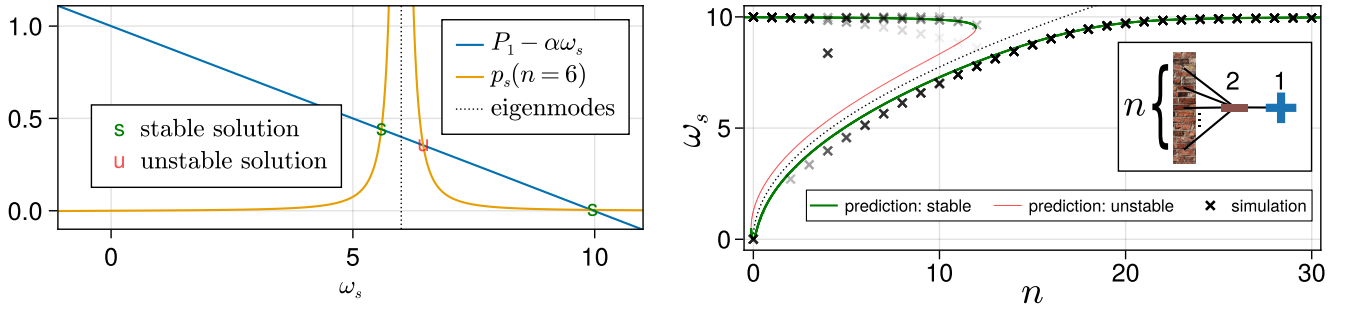


FIG. 3. Network modes shape the landscape of solitary attractor states for the minimal effective model (inset). (left) Intersections between the straight line  $P_1 - \alpha\omega_s$  and the mean energy flow  $p_s(n=6)$  generate stable and unstable solutions according to Eq. (11). We use  $P_1 = 1$ ,  $\alpha = 0.1$ . The single peak of  $p_s$  is centered around the network mode close to  $\sqrt{Kn}$ . (right) Bifurcation diagram with the bifurcation parameter  $n$ . The two stable branches are connected by an unstable branch and centered around the network mode.

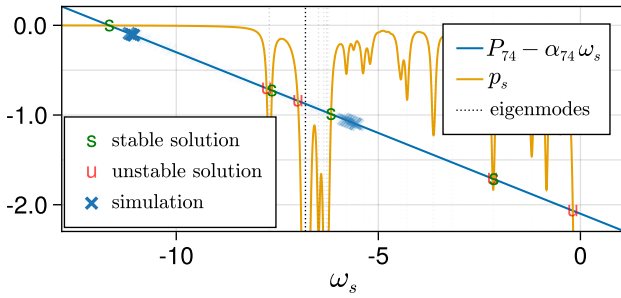


FIG. 4. Solutions of Eq. (11) for a dense sprout node ( $i = 74$ ) in a synthetic power grid (Fig. 2). For the sake of clarity, we slightly modified the node parameters to reduce the number of intersections in the figure (see SM II.C).

to find solitary frequencies in complex networks by solving Eq. (11).

*Acknowledgments.*— Initial investigations of this phenomenon grew out of work by Anton Plietzsch and discussions with Paul Schultz, Chris Bick, Jeroen Lamb, Deniz Eroglu, Tiago Pereira, and Carsten Grabow during a stay at Nesim Mathematics Village.

Part of this work was funded by the DFG grant CoCo-Hype (DFG KU 837/39-2, J.N., J.K., F.H., M.A.).

J.N. gratefully acknowledges support by the Studienstiftung des Deutschen Volkes scholarship foundation and Berlin International Graduate School in Model and Simulation based Research (BIMoS) at Technische Universität Berlin.

- [3] J. A. Acebrón, L. L. Bonilla, C. J. Pérez Vicente, F. Ritort, and R. Spigler, *Reviews of Modern Physics* **77**, 137 (2005).
- [4] L. M. Pecora, F. Sorrentino, A. M. Hagerstrom, T. E. Murphy, and R. Roy, *Nature communications* **5**, 4079 (2014).
- [5] F. A. Rodrigues, T. K. D. M. Peron, P. Ji, and J. Kurths, *Phys. Rep.* **610**, 1 (2016).
- [6] A. Pikovsky, M. Rosenblum, and J. Kurths, *Synchronization: A Universal Concept in Nonlinear Sciences*, Cambridge Nonlinear Science Series (Cambridge University Press, Cambridge, 2001).
- [7] Y. Kuramoto, *Chemical oscillations, waves, and turbulence*, 1984th ed., Springer series in synergetics (Springer, Berlin, Germany, 1984).
- [8] H.-A. Tanaka, A. J. Lichtenberg, and S. Oishi, *Physical Review Letters* **78**, 2104 (1997).
- [9] H.-A. Tanaka, A. J. Lichtenberg, and S. Oishi, *Physica D: Nonlinear Phenomena* **100**, 279 (1997).
- [10] A. Bergen and D. Hill, *IEEE Transactions on Power Apparatus and Systems* **PAS-100**, 25 (1981).
- [11] D. Witthaut, F. Hellmann, J. Kurths, S. Kettemann, H. Meyer-Ortmanns, and M. Timme, *Rev. Mod. Phys.* **94** (2022).
- [12] B. Ermentrout, *Journal of Mathematical Biology* **29**, 571 (1991).
- [13] I. Omelchenko, Y. Maistrenko, P. Hövel, and E. Schöll, *Phys. Rev. Lett.* **106**, 234102 (2011).
- [14] M. Gelbrecht, J. Kurths, and F. Hellmann, *New Journal of Physics* **22**, 033032 (2020).
- [15] L. Halekotte, A. Vanselow, and U. Feudel, *Journal of Physics: Complexity* **2**, 035015 (2021).
- [16] R. Berner, S. Yanchuk, and E. Schöll, *Phys. Rev. E* **103**, 042315 (2021).
- [17] S. Olmi, A. Navas, S. Boccaletti, and A. Torcini, *Physical Review E* **90**, 042905 (2014).
- [18] Y. Maistrenko, B. Penkovsky, and M. Rosenblum, *Phys. Rev. E* **89**, 060901 (2014).
- [19] P. Jaros, Y. Maistrenko, and T. Kapitaniak, *Phys. Rev. E* **91**, 022907 (2015).
- [20] P. J. Menck, J. Heitzig, J. Kurths, and H. Schellnhuber, *Nature Communications* (2014).
- [21] F. Hellmann, P. Schultz, P. Jaros, R. Levchenko, T. Kap-

- [1] S. H. Strogatz, *Physica D: Nonlinear Phenomena* **143**, 1 (2000).
- [2] J. A. Acebrón, L. L. Bonilla, and R. Spigler, *Physical Review E* **62**, 3437 (2000).

- itaniak, J. Kurths, and Y. Maistrenko, Nat. Commun. **11**, 592 (2020).
- [22] P. Jaros, S. Brezetsky, R. Levchenko, D. Dudkowski, T. Kapitaniak, and Y. Maistrenko, Chaos **28**, 011103 (2018).
- [23] J. Nitzbon, P. Schultz, J. Heitzig, J. Kurths, and F. Hellmann, New Journal of Physics **19**, 033029 (2017).
- [24] UCTE, “Final report system disturbance on 4 november 2006,” <https://eepublicdownloads.entsoe.eu/clean-documents/pre2015/publications/ce/otherreports/Final-Report-20070130.pdf>, accessed: 2022-12-19 17:25.
- [25] M. Rohden, A. Sorge, M. Timme, and D. Witthaut, Phys. Rev. Lett. **109**, 064101 (2012).
- [26] X. Zhang, S. Hallerberg, M. Matthiae, D. Witthaut, and M. Timme, Science Advances **5**, eaav1027 (2019).
- [27] P.-J. Menck, *How wires shape volumes*, Ph.D. thesis, Humboldt-Universität zu Berlin, Mathematisch-Naturwissenschaftliche Fakultät I (2014).
- [28] J. Guckenheimer and P. Holmes, *Nonlinear oscillations, dynamical systems, and bifurcations of vector fields*, 1st ed., Applied mathematical sciences (Springer, New York, NY, 2002).
- [29] J. Gao and K. Efsthathiou, Phys. Rev. E **98**, 042201 (2018).
- [30] W. Yue, L. D. Smith, and G. A. Gottwald, Physical Review E **101**, 062213 (2020).
- [31] V. O. Munyayev, M. I. Bolotov, L. A. Smirnov, G. V. Osipov, and I. V. Belykh, Phys. Rev. E **105**, 024203 (2022).
- [32] See Supplemental Material at [URL will be inserted by publisher] for animations of the dynamics of an exemplary complex network; an in-depth, self-contained derivation of our main results; an outline of several possible generalizations; more examples and their comparison; and details of the networks used.
- [33] P. Schultz, J. Heitzig, and J. Kurths, The European Physical Journal Special Topics (2014).
- [34] A. Plietzsch, R. Kogler, S. Auer, J. Merino, A. Gil-de Muro, J. Liße, C. Vogel, and F. Hellmann, SoftwareX **17**, 100861 (2022).
- [35] L. Halekotte and U. Feudel, Scientific Reports **10**, 11783 (2020).
- [36] A. E. Motter, S. A. Myers, M. Anghel, and T. Nishikawa, Nat. Phys. **9**, 191 (2013).
- [37] J. Wassmer, D. Witthaut, and F. Kaiser, Journal of Physics: Complexity **2**, 035003 (2021).
- [38] T. Menara, G. Baggio, D. Bassett, and F. Pasqualetti, Nat. Commun. **13**, 4721 (2022).
- [39] D. Witthaut and M. Timme, New Journal of Physics **14**, 083036 (2012).
- [40] P. Schultz, T. Peron, D. Eroglu, T. Stemler, G. M. Ramírez Ávila, F. A. Rodrigues, and J. Kurths, Phys. Rev. E **93**, 062211 (2016).
- [41] F. Kaiser, V. Latora, and D. Witthaut, Nature Communications **12**, 3143 (2021).
- [42] H. Taher, S. Olmi, and E. Schöll, Phys. Rev. E **100**, 062306 (2019).
- [43] D. Manik, D. Witthaut, B. Schäfer, M. Matthiae, A. Sorge, M. Rohden, E. Katifori, and M. Timme, Eur. Phys. J. Spec. Top. **223**, 2527 (2014).
- [44] V. V. Klinshov, V. I. Nekorkin, and J. Kurths, New Journal of Physics **18**, 013004 (2015).
- [45] R. Kogler, A. Plietzsch, P. Schultz, and F. Hellmann, PRX Energy **1**, 013008 (2022).
- [46] J. Niehues, “Revelations,” <https://gitlab.pik-potsdam.de/jakobn/revelations> (2023).

# Supplementary Material to: Resonant Solitary States in Complex Networks

Jakob Niehues,<sup>1,2,3</sup> S. Yanchuk,<sup>1,2,4</sup> R. Berner,<sup>2</sup> J. Kurths,<sup>1,5</sup> F. Hellmann,<sup>1</sup> and M. Anvari<sup>1,6</sup>

<sup>1</sup>*Potsdam Institute for Climate Impact Research, Telegrafenberg A56, 14473 Potsdam, Germany*

<sup>2</sup>*Humboldt-Universität zu Berlin, Department of Physics, Newtonstraße 15, 12489 Berlin, Germany*

<sup>3</sup>*Technische Universität Berlin, ER 3-2, Hardenbergstrasse 36a, 10623 Berlin, Germany*

<sup>4</sup>*University College Cork, School of Mathematical Sciences, Western Road, Cork, T12 XF62, Ireland*

<sup>5</sup>*Humboldt-Universität zu Berlin, Department of Physics, Newtonstraße 15, 12489 Berlin, Germany*

<sup>6</sup>*Fraunhofer Institute for Algorithms and Scientific Computing, 53757 Sankt Augustin, Germany*

This supplementary material contains a detailed derivation of the central self-consistent equation in the main article. Moreover, we provide details on the examples studied.

## CONTENTS

I. Derivation of the self-consistent equation	1
A. Preliminaries	1
1. Network modes	2
2. Eigenvector localization	2
3. Partition of the system	3
B. Averaging approach	4
C. Linear response	9
D. Validity	10
E. Solitary nodes with several neighbors	10
F. Heterogeneous system parameters	11
G. Several solitary nodes	11
II. Evaluation of the self-consistent equation	12
A. The minimal effective model	12
B. The star graph	13
C. Complex synthetic power grids	14

## I. DERIVATION OF THE SELF-CONSISTENT EQUATION

### A. Preliminaries

We start with a network of  $N$  Kuramoto oscillators with inertia (swing equations),

$$m_i \ddot{\varphi}_i = P_i - \alpha_i \dot{\varphi}_i - \sum_{j=1}^N \kappa_{ij} \sin(\varphi_i - \varphi_j). \quad (\text{S1})$$

A necessary condition for the existence of a steady state is that the driving powers are balanced, that is,  $\sum_{i=1}^N P_i = 0$ . As long as the sum of damping coefficients is not zero, this can always be achieved by shifting to a rotating frame of reference with  $\omega_{\text{ref}} = \frac{\sum_{i=1}^N P_i}{\sum_{i=1}^N \alpha_i}$ . Without loss of generality, we will assume  $\sum_{i=1}^N P_i = 0$  from here on. Alternatively, this can be written as a set of  $2N$  first-order equations,

$$\dot{\varphi}_i = \omega_i, \quad (\text{S2})$$

$$m_i \dot{\omega}_i = P_i - \alpha_i \omega_i - \sum_{j=1}^N \kappa_{ij} \sin(\varphi_i - \varphi_j). \quad (\text{S3})$$

The steady state  $\varphi_i^*$ , i.e.,  $\dot{\varphi}_i = 0$ , is given by the power flow equations,

$$P_i = \sum_{j=1}^N \kappa_{ij} \sin(\varphi_i^* - \varphi_j^*). \quad (\text{S4})$$

### 1. Network modes

The steady state induces a weighted steady-state graph Laplacian

$$\mathcal{L}_{ij} = \begin{cases} \sum_{j,j \neq i}^N \kappa_{ij} \cos(\varphi_i^* - \varphi_j^*) & \text{iff } i = j, \\ -\kappa_{ij} \cos(\varphi_i^* - \varphi_j^*) & \text{iff } i \neq j. \end{cases} \quad (\text{S5})$$

It appears in the linearized dynamics with Jacobian  $\mathcal{J}$ ,

$$\frac{d}{dt} \begin{bmatrix} \mathbf{1} & 0 \\ 0 & \mathcal{M} \end{bmatrix} \begin{bmatrix} \delta\varphi \\ \delta\omega \end{bmatrix} = \mathcal{J} \begin{bmatrix} \delta\varphi \\ \delta\omega \end{bmatrix} = \begin{bmatrix} 0 & \mathbf{1} \\ -\mathcal{L} & -\mathcal{A} \end{bmatrix} \begin{bmatrix} \delta\varphi \\ \delta\omega \end{bmatrix}. \quad (\text{S6})$$

where  $\delta\varphi$  is a vector with entries  $\varphi_i - \varphi_i^*$ , analogously  $\delta\omega$  is a vector with entries  $\omega_i - \omega_i^* = \omega_i$ , and  $\mathcal{M} := \text{diag}(m_i)$ , and  $\mathcal{A} := \text{diag}(\alpha_i)$ .  $\mathcal{L}$  is positive semi-definite, see reference [7]. If the graph is connected, there is exactly one zero eigenvalue. The other eigenvalues are real and positive, and can be ordered  $0 = \Lambda^{[1]} < \Lambda^{[2]} < \dots < \Lambda^{[N]}$ . For  $\mathcal{M} = \mathbf{1}$  and  $\mathcal{A} = \alpha \mathbf{1}^{-1}$ , the eigenvalues of  $\mathcal{J}$  are given by

$$\sigma_{\pm}^{[\ell]} = -\frac{\alpha}{2} \pm \sqrt{\frac{\alpha^2}{4} - \Lambda^{[\ell]}}, \quad (\text{S7})$$

see reference [26]. Since their real parts are negative by assumption <sup>2</sup>, except for one zero eigenvalue, the synchronous state is linearly stable as small perturbations are damped exponentially with time. The imaginary parts of  $\sigma_{\pm}^{[\ell]}$  are the *eigenmodes* of the network, or *network modes*,  $\pm\omega^{[\ell]}$ , that describe oscillations around the fixed point. They are given by  $\omega^{[1]} = 0$  and

$$\omega^{[\ell]} = \sqrt{\Lambda^{[\ell]} - \frac{\alpha^2}{4}}. \quad (\text{S8})$$

for  $\ell = 2, \dots, N$ . We assume that  $\Lambda^{[\ell]} \gg \alpha^2/4$  for  $\ell \geq \ell_{\text{th}}$ , where  $\ell_{\text{th}} \geq 2$  is some threshold. Therefore,  $\omega^{[\ell]} \approx \sqrt{\Lambda^{[\ell]}}$  for  $\ell \geq \ell_{\text{th}}$ .

The components  $V_i^{[\ell]}$  of the corresponding eigenvectors  $\vec{V}^{[\ell]}$  give us the nodal excitation of  $\varphi_i$  of network mode  $\ell$  at node location  $i$ . The zero eigenmode  $\omega^{[1]} = 0$  corresponds to the uniform eigenvector  $V_i^{[1]} = 1/\sqrt{N} \quad \forall i$ . It represents the symmetry of Eq. (S1) under a constant global phase shift. It does not describe an oscillation, but the uniform movement of all phases. Therefore, it is also called *bulk mode*.

### 2. Eigenvector localization

Here, we provide an estimate for the eigenvalue of a highly concentrated steady-state Laplacian eigenvector. It is a typical feature of the networks at hand and will become important in the derivation of the self-consistent equation. Let us assume that a network mode is localized at node  $i$ , or as one could say, its Laplacian eigenvector  $\vec{V}^{[\ell]}$  has a strong support there. We quantify this by

$$\left| \frac{V_j^{[\ell]}}{V_i^{[\ell]}} \right| < \varepsilon_i \quad \forall j \in \mathcal{N}_i, \quad (\text{S9})$$

<sup>1</sup> Note that for homogeneous  $m_i$  and  $\alpha_i$ , one can always be rescaled to 1 by rescaling time.

<sup>2</sup> We only treat networks with linearly stable steady states.



where  $\varepsilon_i$  is a small parameter, and we denote the neighbors of node  $i$  with  $\mathcal{N}_i$ . When evaluated explicitly for component  $i$ , the eigenvector equation yields

$$\Lambda^{[\ell]} V_i^{[\ell]} = \mathcal{L}_{ii} V_i^{[\ell]} + \sum_{j \in \mathcal{N}_i} \mathcal{L}_{ij} V_j^{[\ell]} = \mathcal{L}_{ii} V_i^{[\ell]} - \sum_{j \in \mathcal{N}_i} \kappa_{ij} \cos(\varphi_i^* - \varphi_j^*) V_j^{[\ell]}. \quad (\text{S10})$$

This gives us tight bounds for the value of  $\Lambda^{[\ell]}$ ,

$$\left| \Lambda^{[\ell]} - \mathcal{L}_{ii} \right| = \left| \sum_{j \in \mathcal{N}_i} \kappa_{ij} \cos(\varphi_i^* - \varphi_j^*) \frac{V_j^{[\ell]}}{V_i^{[\ell]}} \right| \leq \mathcal{L}_{ii} \varepsilon_i. \quad (\text{S11})$$

For  $\cos(\varphi_i^* - \varphi_j^*) \approx 1$ , this reduces to

$$\left| \Lambda^{[\ell]} - K_i^* d_i \right| \leq K_i^* d_i \varepsilon_i, \quad (\text{S12})$$

where  $K_i^*$  is the average coupling strength of the links  $\{(i, j) | j \in \mathcal{N}_i\}$  with coupling strenghts  $\{\kappa_{ij}\}$ , and  $d_i = |\mathcal{N}_i|$  is the degree of node  $i$ . We conclude that a highly localized network mode comes with a Laplacian eigenvalue that is closely connected to the degree of the node where the network mode is localized.

### 3. Partition of the system

For the analysis of solitary states, we view the original system as two interacting subsystems, namely, the solitary oscillator  $z$  and the rest, which we denote  $S = \{1, \dots, N\} \setminus z$ , and which forms a synchronized cluster. We assume that node  $z$  is of degree one with neighbor  $k$ . As we show below, the case of several neighbors can be treated analogously due to the additive coupling.

Node  $z$  has a different mean frequency than the synchronized cluster, i.e.,

$$\varphi_z(t) = \omega_s t + \varepsilon \psi_z(t), \quad (\text{S13})$$

where  $\omega_s$  is the time-averaged frequency of node  $z$ ,  $\omega_s := \langle \dot{\varphi}_z \rangle$ ,  $\varepsilon$  a small parameter, and  $\langle \psi_z(t) \rangle = 0$  by assumption. We assume homogeneous inertia  $m$  and damping constants  $\alpha$  for the synchronized cluster  $S$ . We denote the energy flow from node  $i$  to node  $j$  as

$$p_{ij} := \kappa_{ij} \sin(\varphi_i - \varphi_j) = -p_{ji}. \quad (\text{S14})$$

For now, we assume that the solitary oscillator has only one neighbor,  $k$ , without loss of generality. As we show later on, the results can be generalized to several neighbors in a straightforward way due to the additive nature of the coupling via the links from  $z$  to  $k \in \mathcal{N}_z$ .

For the solitary oscillator, we have

$$m_z \ddot{\varphi}_z = P_z - \alpha_z \dot{\varphi}_z - p_{zk}. \quad (\text{S15})$$

We assume that the solitary state is sufficiently close to being periodic with a period that is a multiple of  $T_s := 2\pi/\omega_s$ , hence the energy flows are oscillating functions in time. Regarding the coupling of the two subsystems, we separate the mean energy flow and the oscillating, mean-zero energy flow,

$$p_{zk}(t) := \langle p_{zk} \rangle + p_{zk, \text{osc}}(t). \quad (\text{S16})$$

With the ansatz from Eq. (S13), time averaging of Eq. (S15) yields a self-consistent equation for the solitary mean frequency,

$$0 = Z(\omega_s) := P_z - \alpha_z \omega_s - \langle p_{zk} \rangle. \quad (\text{S17})$$

In order to evaluate Eq. (S17), we need an approximation for  $\langle p_{zk} \rangle$  as a function of  $\omega_s$ , thus closing the equation. By assuming  $\omega_s$  to be generally slowly varying, we can provide the following heuristic dynamical interpretation. The self-consistency function  $Z(\omega_s)$  is the average change in  $m_z \dot{\varphi}_z$  over a period, which needs to be zero for a stable, periodic solitary state. In other words, solutions  $\omega_s$  to  $Z(\omega_s) = 0$  are fixed points  $\omega_s = v^* = \text{const.}$  of the dynamical

system  $\dot{v} = Z(v)$  with state variable  $v$ . Hence, the sign of  $dZ/d\omega_s$  gives us the linear stability of the zeros of  $Z(\omega_s)$ , providing us with a heuristic for the stability of the corresponding periodic orbit with  $\langle \dot{\varphi}_z \rangle = \omega_s$ .

To determine  $\langle p_{zk} \rangle$  as a function of  $\omega_s$ , system parameters and topology, we first need to find an explicit approximation for the trajectory of  $\varphi_k(t)$ , as Eq. (S1) can not be solved analytically.

We start by considering  $\langle p_{zk} \rangle$  and  $p_{zk, \text{osc}}(t)$  one at a time. First, we need to account for the power-imbalance in  $S$ . Eq. (S17) shows that non-zero  $\omega_s$  causes a deviation in  $p_{zk}$  from its value in the synchronous state,  $P_z$ . Furthermore, Fig. 1 in the main article shows that the mean coupling between the solitary node and  $S$  is maximal in the synchronous state, intermediate for intermediate solitary frequency, and approximately zero for natural solitary states. Hence, in a solitary state, where the power in the synchronized cluster is unbalanced, the oscillators in  $S$  perform a slow collective counter-rotation to the solitary node, which can be observed numerically. Adding up Eq. (S1) for the synchronized cluster yields

$$m \frac{d}{dt} \sum_{i \in S} \dot{\varphi}_i = -\alpha \sum_{i \in S} \dot{\varphi}_i - P_z + p_{zk}. \quad (\text{S18})$$

We start by considering only the mean energy flow  $\langle p_{zk} \rangle$  between node  $z$  and the synchronized cluster. Then, the power in the synchronized cluster is unbalanced, and the solution of Eq. (S18) exponentially converges towards

$$\sum_{i \in S} \dot{\varphi}_i = \frac{-P_z + \langle p_{zk} \rangle}{\alpha}. \quad (\text{S19})$$

Therefore, the synchronization frequency of the synchronized cluster is not zero as in the original system, but, on average, lies at

$$\omega_{\text{sync}} := \frac{-P_z + \langle p_{zk} \rangle}{\alpha(N-1)} = -\frac{\alpha_z}{\alpha} \frac{\omega_s}{N-1}, \quad (\text{S20})$$

according to Eq. (S17). Note that for constant ratios  $m_i/\alpha_i$  for all nodes including  $z$ , the  $\alpha_i$ -weighted sum over all frequencies exponentially decays towards zero. Therefore, if  $m_z/\alpha_z = m/\alpha$ , we have  $\alpha_z \omega_s = -\alpha(N-1)\omega_{\text{sync}}$ .

To be able to linearize the dynamics, we need the proper coordinate frame, that eliminates the collective rotation of  $S$ . Therefore, we define the corotating solitary frequency,  $\omega_c := \omega_s - \omega_{\text{sync}}$ . If we shift the phases in the synchronized cluster by  $\omega_{\text{sync}} t$ , the synchronous periodic orbit becomes a fixed point, which induces a steady-state graph Laplacian  $L$ . We assume that it has an eigenvector  $\vec{v}^{[r]}$  with a high concentration at node  $k$ . The corresponding eigenvalue is  $\lambda^{[r]}$ . We observe that this is a typical situation for dense root nodes, which are neighbors of dense sprout nodes. As we show in the preliminaries, the frequency of a highly localized mode is closely connected to the degree of the respective node. We remark that, if such a localized eigenmode does not exist, we can just use the largest eigenmode for the rescaling in the subsequent derivation. Later on, we see that all modes contribute to  $\langle p_{zk} \rangle$ . The magnitude of their contribution depends on their localization at node  $k$  and their frequency.

## B. Averaging approach

Here we derive an explicit expression for Eq. (S17) using the averaging technique. The first step is to rewrite system (S1) so that the fast and slow variables are split with a suitable small parameter  $\varepsilon$ . We consider the case  $\alpha_i = \alpha$  and  $m_i = m$  for all  $i \in S = \{1, \dots, N\} \setminus z$  in the synchronized cluster, and rewrite (S1) by separating the solitary node  $z$  as follows

$$m \ddot{\varphi}_i = P_i - \alpha \dot{\varphi}_i - \sum_{j=1}^N \kappa_{ij} \sin(\varphi_i - \varphi_j), \quad i \in S, \quad (\text{S21})$$

$$m_z \ddot{\varphi}_z = P_z - \alpha_z \dot{\varphi}_z - \kappa_{kz} \sin(\varphi_z - \varphi_k), \quad k \in \mathcal{N}_z. \quad (\text{S22})$$

We first rescale parameters and the time variable<sup>3</sup> using the following ansatz

$$t = \frac{\sqrt{m}}{\nu} t', \quad P_i = \frac{P'_i \alpha \nu}{\sqrt{m}}, \quad \kappa_{ij} = \frac{\kappa'_{ij} \alpha \nu}{\sqrt{m}}, \quad (\text{S23})$$

---

<sup>3</sup> Note that this implies an inverse rescaling of frequencies.

and omitting the prime for the dimensionless quantities (e.g.  $t' \rightarrow t$ ) thereafter. Here  $\nu$  will be specified later. We also introduce the small dimensionless parameter

$$\varepsilon := \frac{\alpha}{\sqrt{m\nu}} \ll 1. \quad (\text{S24})$$

With the rescaling (S23)–(S24), system (S1) transforms into

$$\ddot{\varphi}_i = \varepsilon \left[ P_i - \dot{\varphi}_i - \sum_{j=1}^N \kappa_{ij} \sin(\varphi_i - \varphi_j) \right], \quad i \in S, \quad (\text{S25})$$

$$\ddot{\varphi}_z = \frac{\varepsilon m}{m_z} \left[ P_z - \frac{\alpha_z}{\alpha} \dot{\varphi}_z - \kappa_{zk} \sin(\varphi_z - \varphi_k) \right]. \quad (\text{S26})$$

If  $\varepsilon$  is small, and the terms multiplied by it on the right-hand side are of order one, then the averaging theorem tells us that we have approximately freely rotating oscillators. If we set  $\nu = 1$ , small  $\varepsilon$  means we have a system with very high inertia and low damping. For such a system, this is indeed a good approximate solution. However, it does not describe any coupling between the oscillators.

To obtain the solitary and resonant states we want to describe, we want to consider the case where  $\varepsilon$  is small in part due to  $\nu$ , and  $\nu$  is related to the coupling. If we fix  $\nu^2 \varepsilon \approx 1$  then  $\kappa' \approx \kappa$ , and the right-hand side in (S26) is indeed small. However, there are  $\nu^2$  such that the sum in the right-hand side of (S25) is not small. We will see that these are related to the eigenvalues of the Laplacian of the synchronized cluster. Thus, we proceed to linearize the system near the synchronized cluster.

With  $\delta_{ij}$  as the Kronecker delta, we define shifted power constants

$$\hat{P}_i := P_i - \alpha \omega_{\text{sync}} + \delta_{ik} \langle p_{zk} \rangle = P_i + \frac{\alpha_z \omega_s}{N-1} + \delta_{ik} \langle p_{zk} \rangle. \quad (\text{S27})$$

They are balanced,  $\sum_{i \in S} \hat{P}_i = 0$ . For the phase angles of the synchronized cluster, we make the ansatz

$$\varphi_i(t) = \omega_{\text{sync}} t + \vartheta_i^* + \vartheta_i(t), \quad (\text{S28})$$

where the steady-state of the synchronized cluster with only  $\langle p_{zk} \rangle$  as input is given by  $\vartheta_i(t) = 0$ , and

$$\hat{P}_i = \sum_{j \in S} \kappa_{ij} \sin(\vartheta_i^* - \vartheta_j^*) \quad (\text{S29})$$

are the power flow equations for the steady-state in the synchronized cluster. Equation (S28) can be interpreted as a transformation into the average corotating frame of the synchronized cluster. We define

$$\vartheta_z(t) := \varphi_z(t) - \omega_{\text{sync}} t - \vartheta_k^* = \omega_c t + \varepsilon \psi_z(t) - \vartheta_k^*. \quad (\text{S30})$$

The function  $\psi_z(t)$  is zero with only  $\langle p_{zk} \rangle$  as coupling. The constant phase shift  $\vartheta_k^*$  in  $\vartheta_z(t)$  can be chosen by applying a translation in time and turns out to be a convenient choice later.

Next, we consider also the oscillating part of the energy flow between the two subsystems,  $p_{zk, \text{osc}}(t)$ . With Eq. (S27), the dynamics Eqs. (S25) and (S26) for the corotating coordinates read

$$\ddot{\vartheta}_i = \varepsilon \left[ \hat{P}_i - \dot{\vartheta}_i - \sum_{j=1}^N \kappa_{ij} \sin(\vartheta_i^* + \vartheta_i - \vartheta_j^* - \vartheta_j) \right], \quad \text{for } i \in S \setminus k, \quad (\text{S31})$$

$$\ddot{\vartheta}_k = \varepsilon \left[ \hat{P}_k - \dot{\vartheta}_k - \sum_{j \in S} \kappa_{kj} \sin(\vartheta_k^* + \vartheta_k - \vartheta_j^* - \vartheta_j) + \kappa_{zk} \sin(\vartheta_z - \vartheta_k) - \langle p_{zk} \rangle \right], \quad (\text{S32})$$

$$\ddot{\vartheta}_z = \frac{\varepsilon m}{m_z} \left[ P_z - \frac{\alpha_z}{\alpha} (\dot{\vartheta}_z + \omega_{\text{sync}}) - \kappa_{zk} \sin(\vartheta_z - \vartheta_k) \right]. \quad (\text{S33})$$

We remark that due to the definition of  $\hat{P}_k$ , the last two terms in Eq. (S32) together have zero mean, hence we have successfully eliminated any constant offset in the perturbation induced by the coupling  $p_{zk}$ , which would cause a rotation. We observe that  $\vartheta_k$  is being harmonically driven. Due to the additional nonlinear perturbation  $\vartheta_k \sin \vartheta_z$ , we can not simply apply linear response. Therefore, in the following we apply the averaging theorem to treat this

term and show that it averages out in Eq. (S32). We show later on that one obtains the same result as with the averaging technique, if one neglects this term right away, but in Eq. (S32) only, where it is only a small contribution to the overall coupling of node  $k$ . It should not be ignored in Eq. (S33), as it gives a relevant contribution to  $\langle p_{zk} \rangle$  in Eq. (S17).

Next, we approximate the full energy flow by linearization with respect to  $\vartheta_k$ ,

$$p_{zk} \approx \kappa_{zk} [\sin(\vartheta_z) - \vartheta_k \cos \vartheta_z]. \quad (\text{S34})$$

Using Eq. (S29), we linearize Eqs. (S31) - (S33) with respect to  $\vartheta_i(t)$  for  $i \in S$ ,

$$\ddot{\vartheta}_i = \varepsilon \left[ -\dot{\vartheta}_i - \sum_{j \in S} (\vartheta_i - \vartheta_j) \kappa_{ij} \cos(\vartheta_i^* - \vartheta_j^*) \right] \quad \text{for } i \in S \setminus k, \quad (\text{S35})$$

$$\ddot{\vartheta}_k = \varepsilon \left[ -\dot{\vartheta}_k - \sum_{j \in S} (\vartheta_k - \vartheta_j) \kappa_{kj} \cos(\vartheta_k^* - \vartheta_j^*) + \kappa_{zk} (\sin \vartheta_z - \vartheta_k \cos \vartheta_z) - \langle p_{zk} \rangle \right], \quad (\text{S36})$$

$$\ddot{\vartheta}_z = \frac{\varepsilon m}{m_z} \left[ P_z - \frac{\alpha_z}{\alpha} (\dot{\vartheta}_z + \omega_{\text{sync}}) - (\kappa_{zk} \sin \vartheta_z - \vartheta_k \cos \vartheta_z) \right]. \quad (\text{S37})$$

The steady state in the corotating frame of  $S$  induces a graph Laplacian for the synchronized cluster,

$$L_{ij} := \begin{cases} \sum_{j \in S \setminus i} \kappa_{ij} \cos(\vartheta_i^* - \vartheta_j^*) & \text{iff } i = j, \\ -\kappa_{ij} \cos(\vartheta_i^* - \vartheta_j^*) & \text{iff } i \neq j. \end{cases} \quad (\text{S38})$$

for  $i, j \in S$ . We remark that it is reminiscent of the Laplacian of the original system,  $\mathcal{L}$ , if one removes all entries associated to node  $z$ , i.e., row and column  $z$ , as well as the contribution to  $\mathcal{L}_{kk}$ .

Let  $\vec{\vartheta}$  be the vector with entries  $\vartheta_i$  for  $i \in S$ . We can now write Eqs. (S35) and (S36) in vectorized form,

$$\ddot{\vec{\vartheta}} = \varepsilon \left( -\dot{\vec{\vartheta}} - L\vec{\vartheta} + \vec{f} \right), \quad (\text{S39})$$

$$\vec{f} := \hat{e}_k (\kappa_{zk} \sin \omega_c t - \kappa_{zk} \vartheta_k \cos \omega_c t - \langle p_{zk} \rangle), \quad (\text{S40})$$

where  $\hat{e}_k$  is the Cartesian basis vector in  $k$ -direction, which has components  $\delta_{ik}$ . We have used the zeroth order in  $\varepsilon$  for  $\vartheta_z$ , that is,  $\vartheta_z \approx \omega_c t$ .

We assume that there is a network mode with associated eigenvalue  $\lambda^{[r]}$  that is highly localized at node  $k$ . As shown above, this implies that the associated frequency is closely connected to  $d_k$ , the degree of node  $k$ . We set  $\nu^2 = \lambda^{[r]}$  to measure the systems frequencies in units of  $\sqrt{\lambda^{[r]}}$ . Therefore, the above approximations are most valid for typical root-sprout configurations with highly connected root nodes.

Since  $\kappa'_{ij} = \frac{\kappa_{ij}}{\varepsilon \lambda^{[r]}}$  in Eq. (S23), the Laplacian got rescaled like  $L' = \frac{L}{\varepsilon \lambda^{[r]}}$  (renaming  $L'$  to  $L$  thereafter). We now rescale the Laplacian again, such that we measure it in units of  $\lambda^{[r]}$  and make the  $\varepsilon$ -scaling explicit, that is,  $L' = \frac{L''}{\varepsilon}$ , thus substituting  $L = \frac{L''}{\varepsilon}$  in Eq. (S39), and renaming  $L''$  to  $L$  afterward,

$$\ddot{\vec{\vartheta}} = \varepsilon \left( -\dot{\vec{\vartheta}} + \vec{f} \right) - L\vec{\vartheta}. \quad (\text{S41})$$

We diagonalize the system by transforming into the eigenbasis  $\{\vec{v}^{[\ell]}\}$  of  $L$ ,

$$\vec{\xi} := Q^T \vec{\vartheta}, \quad (\text{S42})$$

$$Q_{ij} := v_i^{[j]}, \quad (\text{S43})$$

$$Q^T L Q := \text{diag}(\lambda^{[\ell]}) := \Gamma, \quad (\text{S44})$$

with the eigenvalues  $\{\lambda^{[\ell]}\}$  ordered by magnitude from  $\ell = 0$  to  $N - 1$ . The  $\xi_\ell$  are the excitations of network modes corresponding to  $\omega^{[\ell]} \approx \sqrt{\lambda^{[\ell]}}$  with their nodal excitations  $\vec{\vartheta}$  distributed across the network according to  $\vec{v}^{[\ell]}$ .

Eq. (S41) becomes

$$\ddot{\vec{\xi}} = \varepsilon \left( -\dot{\vec{\xi}} + \vec{g} \right) - \Gamma \vec{\xi}, \quad (\text{S45})$$

where  $\vec{g} := Q^T \vec{f}$ . Equation (S45) has the form of the perturbation of the Hamiltonian system  $\ddot{\vec{\xi}} = -\Gamma \vec{\xi}$ , where the perturbation is due to the friction term  $\dot{\vec{\xi}}$  and  $\vartheta_z$  in  $\vec{g}$ . The appropriate perturbative approach in this case is averaging [28], where one should first write the system for the slowly varying amplitudes of the network modes, i.e., the amplitudes of the periodic solutions of the unperturbed system. These zeroth order solutions in  $\varepsilon$  of are

$$\xi_\ell(t) = x_\ell \cos(\sqrt{\lambda^{[\ell]}} \cdot t) - z_\ell \sin(\sqrt{\lambda^{[\ell]}} \cdot t), \quad (\text{S46})$$

where  $\vec{x}$  and  $\vec{z}$  are constants specified by initial conditions. Since the zeroth order system is conservative, they describe a set of periodic orbits on tori in phase space. For  $\ell = 1$ , we have  $\lambda^{[1]} = 0$  and an additional constant plus linear motion in time. However, this uniform motion of the synchronized cluster is already accounted for in Eq. (S13) via a global phase shift in the original system, hence we can set it to zero here.

Following reference [28] (theorem 4.1.1, example II), for the first-order solution, we make the ansatz

$$\vec{\xi} = \vec{x}(t) \cos \omega_c t - \vec{z}(t) \sin \omega_c t, \quad (\text{S47})$$

where  $\vec{x}(t)$  and  $\vec{z}(t)$  are now time-dependent amplitude variables. Due to coupling, damping, and resulting resonance between the solitary rotation and the oscillation of the synchronized cluster, the  $\xi_\ell$  slowly move on the solution manifold of the zeroth order system, and the frequency of their collective oscillation is shifted from the Laplacian eigenvalue to  $\omega_s$ .

We write the equations of motion, Eqs. (S45), as a system of first-order differential equations,

$$\frac{d}{dt} \begin{pmatrix} \vec{\xi} \\ \vec{z} \end{pmatrix} := \begin{pmatrix} \vec{\zeta} \\ \varepsilon \left( -\vec{\zeta} + \vec{g} \right) - \Gamma \vec{\xi} \end{pmatrix}, \quad (\text{S48})$$

and transform into a corotating frame with the amplitudes as new variables,

$$\begin{pmatrix} \vec{x} \\ \vec{z} \end{pmatrix} := A(t) \begin{pmatrix} \vec{\xi} \\ \vec{z} \end{pmatrix} := \begin{pmatrix} \mathbb{1} \cos \omega_c t & -\frac{1}{\omega_c} \sin \omega_c t \\ -\mathbb{1} \sin \omega_c t & -\frac{1}{\omega_c} \cos \omega_c t \end{pmatrix} \begin{pmatrix} \vec{\xi} \\ \vec{z} \end{pmatrix}, \quad (\text{S49})$$

using the invertible van der Pol transformation  $A(t)$ , see reference [28] (theorem 4.1.1, example II). The equations of motion for the amplitude variables are

$$\begin{aligned} \frac{d}{dt} \begin{pmatrix} \vec{x} \\ \vec{z} \end{pmatrix} &= \frac{1\omega_c^2 - \Gamma}{\omega_c} \begin{pmatrix} \vec{z} \sin^2 \omega_c t - \vec{x} \cos \omega_c t \sin \omega_c t \\ \vec{z} \cos \omega_c t \sin \omega_c t - \vec{x} \cos^2 \omega_c t \end{pmatrix} \\ &\quad - \frac{\varepsilon}{\omega_c} \begin{pmatrix} \sin \omega_c t (\omega_c \vec{x} \sin \omega_c t + \omega_c \vec{z} \cos \omega_c t + \vec{g}) \\ \cos \omega_c t (\omega_c \vec{x} \sin \omega_c t + \omega_c \vec{z} \cos \omega_c t + \vec{g}) \end{pmatrix}. \end{aligned} \quad (\text{S50})$$

To apply the averaging theorem, we need the right-hand side to be of order  $\varepsilon$ . For the minimal effective model that we discuss below, the synchronized cluster only has a single frequency ( $\Gamma$  is scalar), and we can just assume a close resonance,  $\omega_c^2 - \Gamma = O(\varepsilon)$ . For the networked case, we need to assume one of the following two possibilities for all modes. First, if a mode is in resonance, we have  $\omega_c^2 - \lambda = O(\varepsilon)$ . Second, if the driving frequency is not close to the eigenmode's intrinsic frequency  $\omega^{[\ell]}$ , say  $\omega_c^2 - \lambda = O(1)$ , the mode  $z_\ell$  and  $x_\ell$  will be only weakly excited.

This can be understood heuristically by the observation that in the absence of a resonant excitation, the response will be of the order of the driving force. There are two independent reasons for the driving force to be small, the weak localization of most modes at node  $k$ , and the fact that the driving comes with a factor  $\varepsilon$ .

To make this more explicit, consider the transfer function of Eq. (S45),

$$T(s) = (s^2 + \varepsilon s + \Gamma)^{-1} \quad (\text{S51})$$

$$\tilde{\xi}(s) = \varepsilon T(s) \tilde{g}(s), \quad (\text{S52})$$

where  $\tilde{\xi}(s)$  and  $\tilde{g}(s)$  are the Laplace transforms of  $\vec{\xi}(t)$  and  $\vec{g}(t)$ , respectively. Absence of resonance implies that  $\tilde{g}(s)$  has no support near  $\Gamma$ , and thus  $T(s)g(s)$  is never of order  $\varepsilon^{-1}$ .

We note that this is an additional assumption to example II of the averaging theorem as in reference [28], which does not treat the networked case  $|S| > 1$ . As we show later on, this assumption is self-consistent with the solutions it produces, and with empirically observed behavior of the full system in simulations.

We define the diagonal matrix  $\Delta$  by

$$1\omega_c^2 - \Gamma := \varepsilon \Delta. \quad (\text{S53})$$

Since the system Eq. (S50) is slow moving it is of the right form to apply the averaging theorem in reference [28] (theorem 4.1.1 therein). It states that a system of this form, where the right-hand side is periodic and of order  $\varepsilon$ , can be approximated at order  $O(\varepsilon)$  by an autonomous system which is obtained by time-averaging the right-hand side for fixed (average)  $\vec{x}$  and  $\vec{z}$ . The periodicity is maintained in a  $O(\varepsilon^2)$  term, which we neglect here. The solutions of both systems are  $\varepsilon$ -close for time scales up to  $O(\varepsilon^{-1})$  (in dimensionless time). Translating this back by inverting Eq. (S23), this amounts to time scales of the order  $m/\alpha$ , which is typically much larger than  $T_s = 2\pi/\omega_s$ . Further, hyperbolic fixed points of the averaged system possess a unique hyperbolic orbit in the original system  $\varepsilon$ -close to the fixed point for all  $\varepsilon$  up to some  $\varepsilon_0$ . We make use of the last statement to determine an approximation for the (average) orbit  $\vartheta_k$  from the unique stable fixed point of the averaged system.

By averaging Eq. (S50) over time, we obtain the linear system

$$\frac{d}{dt} \begin{pmatrix} \vec{x} \\ \vec{z} \end{pmatrix} = J \begin{pmatrix} \vec{x} \\ \vec{z} \end{pmatrix} - \vec{h} := -\frac{\varepsilon}{2\omega_c} \begin{pmatrix} \mathbb{1}\omega_c & -\Delta \\ \Delta & \mathbb{1}\omega_c \end{pmatrix} \begin{pmatrix} \vec{x} \\ \vec{z} \end{pmatrix} - \vec{h}, \quad (\text{S54})$$

where the components of the inhomogeneity vector are given by

$$h_\ell = \begin{cases} \frac{\varepsilon\kappa_{zk}}{2\omega_c} v_k^{[\ell]} & \text{for } \ell = 1, \dots, N-1 \\ 0 & \text{for } \ell = N, \dots, 2N-2. \end{cases} \quad (\text{S55})$$

We note that the nonlinear term in  $\vec{g}$  is averaged out, thereby explaining why we can obtain the same result by neglecting it and applying linear response, as shown below. The eigenvalues of the Jacobian  $J$  are given by

$$j_\pm^{[\ell]} = -\frac{\varepsilon}{2} \pm i\frac{\varepsilon\Delta_\ell}{2\omega_c}, \quad (\text{S56})$$

where  $\Delta_\ell$  are diagonal elements of  $\Delta$ . Note that due to its block structure and the invertibility of the blocks, we can easily invert  $J$ . The stable fixed point is located at

$$\begin{pmatrix} \vec{x}^* \\ \vec{z}^* \end{pmatrix} = J^{-1}\vec{h} = -\frac{2}{\varepsilon} \left( \mathbb{1} + \frac{\Delta^2}{\omega_c^2} \right)^{-1} \otimes \begin{pmatrix} \mathbb{1} & \frac{\Delta}{\omega_c} \\ -\frac{\Delta}{\omega_c} & \mathbb{1} \end{pmatrix} \vec{h}, \quad (\text{S57})$$

where in the last expression, the first (diagonal) matrix is to be multiplied with each of the four blocks (also diagonal) in the second matrix, as indicated by the symbol  $\otimes$ . The fixed point solution for the components of  $\vec{\xi}$  lies at

$$\xi_\ell = x_\ell^* \cos \omega_c t - z_\ell^* \sin \omega_c t = -\frac{\kappa_{zk}\omega_c}{\omega_c^2 + \Delta_\ell^2} v_k^{[\ell]} \cos \omega_c t - \frac{\kappa_{zk}\Delta_\ell}{\omega_c^2 + \Delta_\ell^2} v_k^{[\ell]} \sin \omega_c t. \quad (\text{S58})$$

With Eqs. (S34), (S42) and (S58), and the zeroth order approximation of  $\vartheta_z$ , we can now evaluate Eq. (S17),

$$0 = Z(\omega_s) := P_z - \alpha_z \omega_s - \frac{\kappa_{zk}^2}{2} \sum_{\ell=1}^{N-1} \frac{\alpha \omega_c \left( v_k^{[\ell]} \right)^2}{\left( \lambda^{[\ell]} - m\omega_c^2 \right)^2 + \alpha^2 \omega_c^2}. \quad (\text{S59})$$

Note that we have already re-substituted  $\Delta_\ell$  and the original parameters by inverting Eq. (S23). Following Eq. (S20), the corotating solitary frequency  $\omega_c$  can be expressed by

$$\omega_c = \left( 1 + \frac{\alpha_z}{\alpha} \frac{1}{N-1} \right) \omega_s. \quad (\text{S60})$$

We assume that  $\alpha_z$  and  $\alpha$  are of similar magnitude, hence for very large  $N$ , one could approximate  $\omega_c \approx \omega_s$ , however, we keep the more general form. Since the Laplacian given in Eq. (S38) and its eigenvectors and eigenvalues depend on  $\langle p_{zk} \rangle$ , we need to approximate it, in order to evaluate Eq. (S59). We assume that the dependence is weak, and choose to use the steady-state phase angles  $\varphi_i^*$  determined by Eq. (S4) instead of  $\vartheta_i^*$  (for  $i \in S$ ). Alternatively, one could omit  $\langle p_{zk} \rangle$  in the definition of  $\hat{P}_i$ , and  $\omega_{\text{sync}}$  when evaluating Eqs. (S20), (S27) and (S38). Given an approximation of the Laplacian, Eq. (S60) closes Eq. (S59), which can be evaluated numerically to find solutions for  $\omega_s$ . In principle, the solutions can be used to increase the accuracy of the approximation of the Laplacian, leading to an iterative solution algorithm. Here, we evaluate the zeroth-order solutions of this cycle, as they are already accurate.  $L$  is then obtained by omitting column and line  $z$  from the  $N \times N$  Laplacian of the total system  $\mathcal{L}$ , and omitting the term in  $\mathcal{L}_{kk}$  that stems from the coupling between nodes  $k$  and  $z$  as well. This last steps conserves the Laplacian property. Without

this last step, due to the Poincaré separation theorem, the eigenvalues of  $L$  lie between those of  $\mathcal{L}$ . We suspect that something similar holds, at least approximately, when including the correction of the diagonal entry  $\mathcal{L}_{kk}$ .

The zeros of Eq. (S59) give rise to approximate solutions of the dynamics in Eq. (S1) with  $\langle \dot{\varphi}_z \rangle = \omega_s$ . The linear stability of a solution  $\omega_s$  of  $Z(\omega_s) = 0$  is given by  $dZ/d\omega_s < 0$ , which is equivalent to

$$\begin{aligned} \alpha_z &< -\frac{d\langle p_{zk} \rangle}{d\omega_s} = -\frac{d\langle p_{zk} \rangle}{d\omega_c} \times \frac{d\omega_c}{d\omega_s} \\ &= \sum_{\ell=1}^{N-1} \kappa_{zk}^2 \alpha \left( v_k^{[\ell]} \right)^2 \frac{(\lambda^{[\ell]} - m\omega_c^2)^2 + \alpha^2 \omega_c^2 + 2\omega_c^2 [2m(\lambda^{[\ell]} - m\omega_c^2) - \alpha^2 \omega_c]}{2 \left[ (\lambda^{[\ell]} - m\omega_c^2)^2 + \alpha^2 \omega_c^2 \right]^2} \\ &\quad \times \left( 1 + \frac{\alpha_z}{\alpha} \frac{1}{N-1} \right). \end{aligned} \quad (\text{S61})$$

Graphically, this means that the curve  $\langle p_{zk} \rangle(\omega_s)$  intersects the straight line  $P_z - \alpha_z \omega_s$  with a slope greater than  $-\alpha_z$ , i.e., coming from below in positive  $\omega_s$ -direction.

### C. Linear response

Here, we provide a second derivation of Eq. (S59) with a heuristic, but intuitive method that relies on linear response, cf. reference [26]. If we split the linearized energy flow in Eq. (S34) in its mean and oscillating part, cf. Eq. (S16), we can approximate

$$p_{zk, \text{osc}}(t) \approx \kappa_{zk} \sin \omega_c t, \quad (\text{S62})$$

in Eq. S32) for small  $\vartheta_k$ . This is valid, if the neglected nonlinear term  $\vartheta_k \sin \vartheta_z$  is only a small contribution to the overall coupling of  $\vartheta_k$ . As noted before, the term should not be neglected in Eq. S33), where it is the only coupling term and crucial for nonzero  $\langle p_{zk} \rangle$  in Eq. (S17).

Now with only harmonic forcing, we can apply linear response. Defining  $\chi_i := \omega_i - \omega_{\text{sync}} = \dot{\vartheta}_i$ , Eq. (S3) for the synchronized cluster transforms into

$$m\dot{\chi}_i \approx \hat{P}_i - \alpha\chi_i - \sum_{j \in S} \kappa_{ij} \sin(\vartheta_i - \vartheta_j) + \delta_{ik} \kappa_{kz} \sin(\omega_c t). \quad (\text{S63})$$

We linearize with respect to the  $\vartheta_i$  around  $\vartheta_i^*$ , and solve for them using linear response with the ansatz

$$\vartheta_i = \vartheta_i^* + \kappa_{kz} \theta_i + \kappa_{kz} \vartheta_i^{(k)}(t). \quad (\text{S64})$$

Here,  $\theta_i$  is the constant part, and  $\vartheta_i^{(k)}(t)$  the time-varying part of the response. The external perturbing signal is the sinusoid with amplitude  $\kappa_{kz}$  and frequency  $\omega_c$ . We write it as a vector  $\vec{F}^{(k)}(t)$  with components  $\delta_{ik} \kappa_{kz} \Im(e^{i\omega_c t})$ , where  $\Im$  is the imaginary part. The linearized system in vectorized form reads

$$m\dot{\vec{\chi}} = \alpha \vec{\chi} - L \kappa_{kz} \vec{\vartheta}^{(k)} + \vec{F}^{(k)}(t). \quad (\text{S65})$$

Zhang et al. show that the linear response is valid for amplitudes of this magnitude, see reference [26]. Following their calculation, the constant parts of the response are the same,  $\theta_i = \theta$  for all  $i$ , and fall out of the equation, while the time-varying part of the response is

$$\kappa_{kz} \vec{\vartheta}^{(k)}(t) = \Im \left[ (L - m\omega_c^2 + i\alpha\omega_c)^{-1} \times \vec{F}^{(k)}(t) \right]. \quad (\text{S66})$$

An analytical expression is obtained by projecting  $\vec{F}^{(k)}(t)$  onto the orthonormal eigenbasis of  $L$ , i.e., inserting  $\mathbb{1}_{ij} = \sum_{\ell=1}^{N-1} v_i^{[\ell]} \left( v_j^{[\ell]} \right)^T$ ,

$$\kappa_{kz} \vec{\vartheta}^{(k)}(t) = \Im \left( \sum_{\ell=1}^{N-1} \frac{\vec{v}^{[\ell]} v_k^{[\ell]}}{\lambda^{[\ell]} - m\omega_c^2 + i\alpha\omega_c} \kappa_{kz} e^{i\omega_c t} \right). \quad (\text{S67})$$

If we define the modal response amplitudes at node  $i$  as

$$a_i^{(k)[\ell]} := \frac{\kappa_{kz} v_i^{[\ell]} v_k^{[\ell]}}{\sqrt{(\lambda^{[\ell]} - m\omega_c^2)^2 + \alpha^2 \omega_c^2}}, \quad (\text{S68})$$

and the modal phase lags  $\delta^{[\ell]}$  as

$$\begin{aligned} \tan \delta^{[\ell]} &:= -\frac{\alpha \omega_c}{\lambda^{[\ell]} - m\omega_c^2}, \\ \sin \delta^{[\ell]} &= -\frac{\alpha \omega_c}{\sqrt{(\lambda^{[\ell]} - m\omega_c^2)^2 + \alpha^2 \omega_c^2}}, \\ \cos \delta^{[\ell]} &= \frac{\lambda^{[\ell]} - m\omega_c^2}{\sqrt{(\lambda^{[\ell]} - m\omega_c^2)^2 + \alpha^2 \omega_c^2}}, \end{aligned} \quad (\text{S69})$$

we can write the response as

$$\kappa_{kz} \vartheta_i^{(k)}(t) = \Im \left[ a_i^{(k)[\ell]} e^{i(\omega_c t + \delta^{[\ell]})} \right]. \quad (\text{S70})$$

This provides us with the following interpretation. The solitary rotation with frequency  $\omega_c$  excites network modes given by  $\omega^{[\ell]} \approx \sqrt{\lambda^{[\ell]}}$ . The nodal amplitudes depend on the mismatch between the driving frequency  $\omega_s$  and the eigenfrequencies of the network, as well as the localization of the corresponding eigenvectors and the damping.

To close the self-consistent equation, we need to determine how the excitation of the network acts back on  $\omega_c$ . Averaging over  $\dot{\omega}_z$ , see Eq. (S17), using Eqs. (S34) and (S70) and  $\vartheta_z \approx \omega_c t$ , yields the same self-consistent equation as the averaging approach, Eq. (S59). In terms of the response amplitudes and phase lags, the self-consistency function takes the form

$$Z(\omega_s) = P_z - \alpha_z \omega_s + \frac{\kappa_{kz}}{2} \sum_{\ell=1}^N a_k^{(k)[\ell]} \sin \delta^{[\ell]}. \quad (\text{S71})$$

In fact, the terms in the denominators in the sum over all modes in Eq. (S59) resemble the resonance curve of linear oscillators. It is known as Cauchy–Lorentz distribution, Lorentz(ian) function, or Breit–Wigner distribution.

#### D. Validity

The derivation is based on system parameters and topologies that result in small  $\varepsilon$  and localized eigenmodes, which is always given in our examples. Precise but concise general statements of the validity range of our theory would be difficult to obtain. To test the fulfillment of assumptions, one could compare the approximation of the trajectories from Eqs. (S34), (S42) and (S58) or statistics obtained from those with simulations. The same goes for Eq. (S70). Note that an approximation of  $\vartheta_z$  as in S30 can be obtained by approximation and integration of S37. See reference [48] for some examples. We observe that the self-consistent equation tends to have no solutions in some regimes where it is not valid, see reference [48].

#### E. Solitary nodes with several neighbors

In the previous derivations, we assumed that the solitary node is of degree one with the neighbor  $k$ . If the solitary node has a higher degree, we can generalize the self-consistent equation as follows. Due to linearity, we can simply superpose the perturbations entering the network through the links from the solitary node to its neighbors  $k \in \mathcal{N}_z$ . This transforms Eq. (S15) into

$$m_z \ddot{\varphi}_z = P_z - \alpha_z \dot{\varphi}_z - \sum_{k \in \mathcal{N}_z} p_{zk}, \quad (\text{S72})$$

i.e., replacing  $p_{zk}$  by  $p_z := \sum_k p_{zk}$  from there on. For the averaging approach, this corresponds to an additional sum over  $k \in \mathcal{N}_z$  in Eq. (S55) and thereafter. For the linear response, we sum over several perturbation vectors in



Eqs. (S63) to (S65). The result is

$$0 = Z(\omega_s) := P_z - \alpha_z \omega_s - \sum_{k \in \mathcal{N}_z} \frac{\kappa_{zk}^2}{2} \sum_{\ell=1}^{N-1} \frac{\alpha \omega_c \left(v_k^{[\ell]}\right)^2}{\left(\lambda^{[\ell]} - m \omega_c^2\right)^2 + \alpha^2 \omega_c^2}. \quad (\text{S73})$$

Eq. (S61) also gets an additional sum over  $k \in \mathcal{N}_z$ .

### F. Heterogeneous system parameters

So far, we assumed that the synchronized cluster has homogeneous inertia  $m_i = m$  and damping  $\alpha_i = \alpha$  for  $i \in S$ , while allowing for different parameters  $m_z$  and  $\alpha_z$  at the solitary node, as well as heterogeneity in the power constants  $P_i$  and coupling matrix  $\kappa_{ij}$  for the whole network. If one allows generally heterogeneous inertia and damping in the whole network, the self-consistent equation can still be evaluated numerically<sup>4</sup>, as outlined below.

To see this, consider Eq. (S66) and replace  $m$  by  $M := \text{diag}(m_i)$  and  $\alpha$  by  $A := \text{diag}(\alpha_i)$  for  $i \in S$ . If  $M$ ,  $A$  and  $L$  do not commute<sup>5</sup>, they can not be diagonalized simultaneously and the projection onto  $L$ 's eigenbasis of network modes can not be applied to invert the matrix

$$R^{-1}(\omega_c) := L - \omega_c^2 M + \omega_c A. \quad (\text{S74})$$

However, this can still be done numerically. Multiplication of the *response matrix*  $R(\omega_c)$  with  $\vec{F}^{(k)}(t)$ , taking the imaginary part, projecting out component  $k$  to get  $\vartheta_k^{(k)}(t)$ , and time-averaging Eq.(S34), which is a projection on the  $\kappa_{zk} \cos \omega_c t$  function, all amount to taking the matrix element  $-\frac{\kappa_{zk}^2}{2} \Im(R_{kk})$  for each solitary neighbor  $k \in \mathcal{N}_z$ . Hence, the self-consistent equation can be written as

$$0 = Z(\omega_s) := P_z - \alpha_z \omega_s + \sum_{k \in \mathcal{N}_z} \frac{\kappa_{zk}^2}{2} \Im[R_{kk}(\omega_c)]. \quad (\text{S75})$$

Note that, here,  $\omega_{\text{sync}}$  does not obey Eq. (S20), but the following generalized version. Averaging over Eq. (S18) with the ansatz  $\langle \dot{\varphi}_i \rangle = \omega_{\text{sync}}$  for  $i \in S$  yields

$$\omega_{\text{sync}} = \frac{-P_z + \langle p_z \rangle}{\sum_{i \in S} \alpha_i} = \frac{-\omega_s \alpha_z}{\sum_{i \in S} \alpha_i} = -\frac{\alpha_z}{\alpha^*} \frac{\omega_s}{N-1}, \quad (\text{S76})$$

where  $\alpha^*$  is the average  $\alpha_i$  in the synchronized cluster, and

$$\omega_c := \omega_s - \omega_{\text{sync}} = \left(1 + \frac{\alpha_z}{\sum_{i \in S} \alpha_i}\right) \omega_s = \left(1 + \frac{\alpha_z}{\alpha^*} \frac{1}{N-1}\right) \omega_s. \quad (\text{S77})$$

We expect that the mechanism behind the solitary frequency tuning in heterogeneous networks is still resonance with network modes, as was the case for homogeneous networks. The modes are still the imaginary parts of the Jacobian's eigenvalues in Eq. (S6), however, a simple relationship to the eigenvalues of the Laplacian like Eq. (S7) does not hold anymore. We reserve it for future work to test Eq. (S75) for heterogeneous  $M$  and  $A$ .

### G. Several solitary nodes

The self-consistency framework presented in this work can be generalized from 1-solitary states to  $l$ -solitary states with  $l$  nodes that oscillate around desynchronized frequencies. If all  $l$  nodes have different frequencies, they do not interact with each other directly, because their coupling cancels out. However, they all excite network modes, and we can superpose the respective responses of the synchronized cluster, which has size  $N-l$  now. Analogous to the considerations in this work, we can get a set of  $l$  self-consistent equations that are only weakly coupled through  $\omega_{\text{sync}}$ , because averaging over the equations for  $\dot{\varphi}_l$  averages out the responses to frequencies other than the respective  $\omega_{c;l}$ .

<sup>4</sup> Note that numerical computation of the eigenvectors and eigenvalues of the Laplacian is necessary for complex networks, anyway. Numerical evaluation of the zeros of the self-consistent equation is necessary for networks as complex as the star graph, already.

<sup>5</sup> As Jörg Liesen pointed out in personal correspondence, for a general connected graph Laplacian, the only commuting diagonal matrix of the Laplacian is the identity up to a scalar multiplicative constant.

If solitary nodes have identical frequencies, we enter the regime of cluster synchronization. When averaging over the equations for  $\dot{\varphi}_l$ , the response of the network to all identical frequencies add up in every respective equation. One has to take care of additional constant phase shifts between the members of the cluster<sup>6</sup>. In this work, only concerned with 1-solitaries, this could be ignored due to the averaging process.

We expect that there are limits to the amount of perturbations and responses that can be superposed, because the assumption that linearization works might break down at some point. It is a task for future work to explore the capabilities and limits of extensions of the theory of solitary states presented here.

## II. EVALUATION OF THE SELF-CONSISTENT EQUATION

Starting from the self-consistent equation, Eq. (S59), one can apply model reduction by simply replacing the Laplacian eigenvalues and eigenvectors with the ones from effective models. In the following, we evaluate several effective models and a complex network without any reduction as examples.

### A. The minimal effective model

The minimal effective model is the simplest model that shows tristability between the synchronous state and solitary states at several frequencies. The graph of the minimal effective model can be seen in the inset in Fig. 3 (right) in the main article. Starting from a network with dense a sprout node,  $z$ , and root node,  $k$ , we rewrite the dynamics using the local order parameter of node  $k$ ,

$$\rho_k e^{i\Psi_k} := \frac{1}{\kappa_{kz}^* n} \sum_{j \in \mathcal{N}_k} \kappa_{kj} e^{i\varphi_j}, \quad (\text{S78})$$

where

$$\kappa_{kz}^* n := \sum_{j \in \mathcal{N}_k} \kappa_{kj}, \quad (\text{S79})$$

so that  $\kappa_{kz}^*$  is the mean coupling strength of the links adjacent to node  $k$  except the link  $(k, z)$ . This is inspired by the classical Kuramoto order parameter, see reference [8]. Now we can rewrite Eq. (S3) for node  $k$ ,

$$m\dot{\omega}_k = P_k - \alpha\omega_k - \kappa_{kz} \sin(\varphi_k - \omega_s t) - \rho_k \kappa_{kz}^* n \sin(\varphi_k - \Psi_k). \quad (\text{S80})$$

The complex network is then reduced to a slack node<sup>7</sup> and the two nodes  $z$  and  $k$  by setting the inertia of the rest of the grid to infinity. This is especially accurate for large, well-synchronized networks. The frequencies of the nodes in the synchronized cluster are zero and their phases constant. Without loss of generality, we set  $\Psi_k = 0$ . We approximate  $\rho_k$  by its asymptotic temporal mean value  $\langle \rho_k \rangle$ . Between the root and the slack node, there are  $n$  lines of coupling strength  $K$ . Due to incoherence of the nodes in  $\mathcal{N}_k$ , we know that  $\rho_k < 1$ . This leads to an effective coupling strength  $\langle \rho_k \rangle \kappa_{kz}^* n$ , which is smaller than in the idealized case with  $\kappa_{kz}^* n$ . Therefore, we expect resonances at smaller  $\omega_s$  in complex networks. For the analysis of the minimal effective model, we label the sprout node  $z = 1$ , the root node  $k = 2$ , and define  $K_1 := \kappa_{12}$ ,  $K_2 := \kappa_{21}$ , and set  $K_3 n := \kappa_{kz}^* n \langle \rho_k \rangle$ .

The equations of motion of the minimal effective model are

$$m_1 \ddot{\varphi}_1 = P_1 - \alpha_1 \dot{\varphi}_1 - K_1 \sin(\varphi_1 - \varphi_2), \quad (\text{S81})$$

$$m_2 \ddot{\varphi}_2 = P_2 - \alpha_2 \dot{\varphi}_2 - K_2 \sin(\varphi_2 - \varphi_1) - K_3 n \sin \varphi_2. \quad (\text{S82})$$

We set  $m_1 = m_2 = 1$ ,  $P_1 = 1 = -P_2$ ,  $\alpha_1 = \alpha_2 = 0.1$ , and  $K = 6$ . In a power grid context,  $K_1 = K_2 = K$ ; furthermore,  $n$  gives us the freedom to set  $K_3 = K$ , too. However, this system can be analyzed in a more general form. For the slack node, we just have  $\varphi_3 = 0$  at all times. Node 1 can have different solitary frequencies, while node 2 and 3 form the synchronized cluster<sup>8</sup>. Due to the presence of a slack node in the synchronized cluster, we have  $\omega_{\text{sync}} = 0$ , hence  $\omega_c = \omega_s$ . Effectively,  $\varphi_3$  does not appear in the equations of motion, and the synchronized cluster only contains node

<sup>6</sup> Note that the system of  $l$  equations determines  $\omega_s$  and  $l - 1$  relative phases, as we can fix one.

<sup>7</sup> A slack node has infinite mass and fixed phase. It is also called infinite-grid node. It can absorb any amount of power instantaneously and is widely used in engineering to balance systems.

<sup>8</sup> Node 2 can also be solitary at its natural frequency, but we focus on node 1, for which this toy model is designed.

2. The steady state is given by  $\varphi_2 = 0$ . The Laplacian and its eigenvectors and eigenvalues are scalars,  $L = K_3 n$ ,  $\vec{v} = 1$ ,  $\lambda = L$ . The self-consistent equation reads

$$0 = P_1 - \alpha_1 \omega_s \cdot \left( 1 + \frac{\alpha_2}{2\alpha_1} \frac{K_1 K_2 \alpha_2}{(K_3 n - m_2 \omega_s^2)^2 + \alpha_2^2 \omega_s^2} \right). \quad (\text{S83})$$

We see that  $0 < |\omega_s| < |\Omega_1|$ . Furthermore, the self-consistency condition is symmetric under  $\omega_s \rightarrow \omega_s$  while  $P_1 \rightarrow -P_1$ . The conditions can be solved for  $n$  explicitly, revealing two branches that are horizontally centered around  $\omega_s = \text{sign}(P_1) \sqrt{\lambda/m_2}$  in the  $\omega_s$ - $n$ -plane,

$$n_{\pm} = \frac{m_2 \omega_s^2}{K_3} \pm \sqrt{\frac{\alpha_2 K_1 K_2}{2\alpha_1 K_3^2} \frac{\omega_s}{\Omega_1 - \omega_s} - \frac{\alpha_2^2 \omega_s^2}{K_2^2}}. \quad (\text{S84})$$

The  $\omega_+ = \omega_s(n_+)$  branch is stable, while the  $\omega_-$  branch has stable and unstable parts, see Fig. 3 in the main article.

## B. The star graph

A more detailed model replaces the slack node in the minimal effective model by  $n$  identical nodes with zero power generation to mimic a synchronized power-balanced grid connected that is well-connected to the root node. The resulting star-shaped graph with  $2 + n$  nodes is shown in the inset in Fig. S1 (right). The equations of motion are

$$m_1 \dot{\omega}_1 = P_1 - \alpha_1 \omega_1 - \kappa_{12} \sin(\varphi_1 - \varphi_2), \quad (\text{S85})$$

$$m_2 \dot{\omega}_2 = P_2 - \alpha_2 \omega_2 - \kappa_{21} \sin(\varphi_2 - \varphi_1) - \sum_{j=3}^{2+n} \kappa_{2j} \sin(\varphi_2 - \varphi_j), \quad (\text{S86})$$

$$m_i \dot{\omega}_i = P_i - \alpha_i \omega_i - \kappa_{i2} \sin(\varphi_i - \varphi_2) \quad \text{for } i \in \{3, \dots, 2+n\}. \quad (\text{S87})$$

For identical  $\varphi_{i \geq 3}$ , the latter two equations of motion can be reduced to

$$m_2 \dot{\omega}_2 = P_2 - \alpha_2 \omega_2 - \kappa_{21} \sin(\varphi_2 - \varphi_1) - \kappa_{23} n \sin(\varphi_2 - \varphi_3), \quad (\text{S88})$$

$$m_3 \dot{\omega}_3 = P_3 - \alpha_3 \omega_3 - \kappa_{32} \sin(\varphi_3 - \varphi_2). \quad (\text{S89})$$

Again, we use identical  $m_i = m = 1$ ,  $\alpha_i = \alpha = 0.1$  and  $\kappa_{ij} = 6$  (if connected). The power constants are given by  $P_1 = -P_2 = 1$ , and  $P_3 = 0$ . We observe that node 3 does not have solitary states, because  $P_3 = 0$ . Any initial difference in the  $\varphi_{i \geq 3}$  are dissipated over time, which makes any additional links between these nodes obsolete. For example, simulations of a network with additional all-to-all coupling except for node 1, show the same asymptotic behavior.

The steady state of the original network, including node 1, is given by  $P_1 = K \sin(\varphi_1^* - \varphi_2^*)$  and  $0 = P_3 = K \sin(\varphi_3^* - \varphi_2^*)$ . The synchronized cluster has the  $(1+n) \times (1+n)$  steady-state Laplacian

$$L = K \begin{bmatrix} n & -1 & -1 & \dots & -1 \\ -1 & 1 & 0 & \dots & 0 \\ -1 & 0 & 1 & \ddots & \vdots \\ \vdots & \vdots & \ddots & \ddots & 0 \\ -1 & 0 & \dots & 0 & 1 \end{bmatrix}. \quad (\text{S90})$$

Its eigenvalues and eigenvectors are

$$\{\lambda^{[\ell]}\} = K \cdot \{0, 1, \dots, 1, n+1\}, \quad (\text{S91})$$

$$v_i^{[1]} = \frac{1}{\sqrt{n+1}}, \quad v_i^{[n+1]} = \frac{1 - \delta_{i1}(n+1)}{\sqrt{n^2 + n}}. \quad (\text{S92})$$

The eigenvectors to the  $n-1$  eigenvalues  $K$  do not contribute to the self-consistent equation for solitary node 1, because they are strictly zero at the neighbor, node 2. They can be obtained by orthogonalization of

$$\tilde{v}_i^{[\ell]} = \frac{\delta_{i2} - \delta_{i(\ell+1)}}{\sqrt{2}} \quad \text{for } \ell = 2, \dots, n. \quad (\text{S93})$$

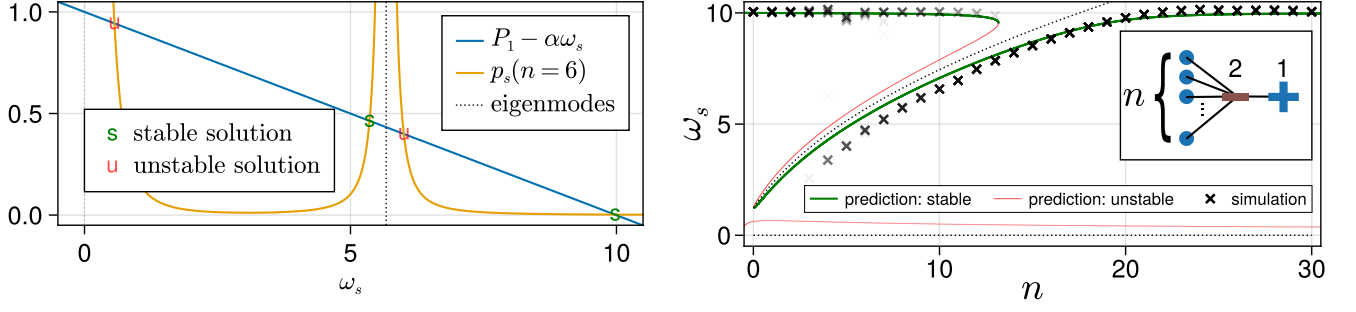


FIG. S1. How network modes shape the landscape of solitary attractor states for a star-shaped graph, cf. Fig. 3 in the main article. (left) Intersections between the straight line  $P_1 - \alpha\omega_s$  and the mean energy flow  $p_s(n=6)$  generate stable and unstable solutions according to Eq. (S59). We use  $P_1 = 1$ ,  $\alpha = 0.1$ . The single non-zero peak of  $p_s$  is centered around the network mode close to  $\sqrt{K(n+1)}$ . (right) Bifurcation diagram with bifurcation parameter  $n$ . The inset shows the graph. Round nodes have  $P_i = 0$ . We plot the asymptotic frequencies obtained from simulations of random initial conditions.

Note that component  $i$  of the eigenvectors corresponds to  $\varphi_{i+1}$  in the original graph.

Eq. (S59) explicitly evaluates to

$$Z(\omega_s) = P_1 - \alpha_1\omega_s - \frac{K^2\alpha\omega_c}{2} \left( \frac{\frac{1}{n+1}}{(m\omega_c^2)^2 + \alpha^2\omega_c^2} + \frac{\frac{n}{n+1}}{(K(n+1) - m\omega_c^2)^2 + \alpha^2\omega_c^2} \right), \quad (\text{S94})$$

where  $\omega_c$  is given by Eq. (S60). The solutions and their linear stability are shown for  $n = 6$  in Fig. S1 (left). The bifurcation diagram is shown in the right panel. In comparison to the minimal effective model in Fig. 3 in the main article, we see here that Eq. (S59) for any network with a synchronized cluster of size larger than one (not counting infinite-grid nodes) has an additional unstable solution due to the bulk mode at  $\lambda^{[1]} = 0$ . Other than that, the features are similar to the minimal effective model. However, the only contributing non-zero network mode lies close to  $\lambda^{[n+1]} = K(n+1)$ .

Note that the network modes that are shown are translated into the static frame via

$$\mu^{[\ell]} := \text{sign}(P_1) \cdot \left( 1 + \frac{\alpha_z}{\alpha} \frac{1}{N-1} \right)^{-1} \sqrt{\frac{\lambda^{[\ell]}}{m}}, \quad (\text{S95})$$

cf. Eq. (S60). The reason is that  $\omega_c$  is in resonance with  $\sqrt{\lambda^{[\ell]}}$ , such that  $\lambda^{[\ell]} - m\omega_c^2$  becomes small and  $\text{sign}(\omega_s) = \text{sign}(\omega_c) = \text{sign}(P_1)$ . However, we plot  $\omega_s$ , for which the original network modes  $\pm\sqrt{\lambda^{[\ell]}}/m$  appear shifted away from the peaks.

### C. Complex synthetic power grids

Fig. S2 shows the graph of a spatially embedded synthetic power grid.

Fig. S3 shows properties of the ensemble of 100 synthetic power grids with  $N = 100$  nodes each.

Fig. S4 shows all asymptotic frequencies and a histogram of the number of desynchronized nodes for grid 1.

Fig. S5 shows the solutions of Eq. (S59) for  $z = 74$  and homogeneous parameters  $P_i = \pm 1$  and  $\alpha_i = 0.1$  for the solitary oscillator ( $P_{74} = -1$ ) and all other oscillators. Fig. 4 in the main article shows the same, but for  $P_{74} = -1 + \Delta P$  with  $\Delta P = -1.1$  and  $\alpha_{74} = 0.18$ . The other  $P_i$  are shifted from their standard values  $\pm 1$  by  $-\Delta P/N$  to maintain power balance. This slight adjustment makes the analytical predictions in the figure much clearer. The simulations confirm that the dynamics, especially the locations and stability of the solitary states, are virtually unchanged.

Fig. S6 shows the solutions of Eq. (S59) for node 75, which is a generator<sup>9</sup>. This illustrates that these intersection plots are point-symmetric with respect to the origin if consumers and generators are exchanged. This corresponds to the symmetry of Eq. (S59) under  $P_z \rightarrow -P_z$  while  $\omega_s \rightarrow -\omega_s$ , which implies  $\omega_c \rightarrow -\omega_c$ . We remark that due to other

<sup>9</sup> Note that the visibilities (alpha values) of the simulation data points are not comparable between plots due to normalization and manual increase if necessary.

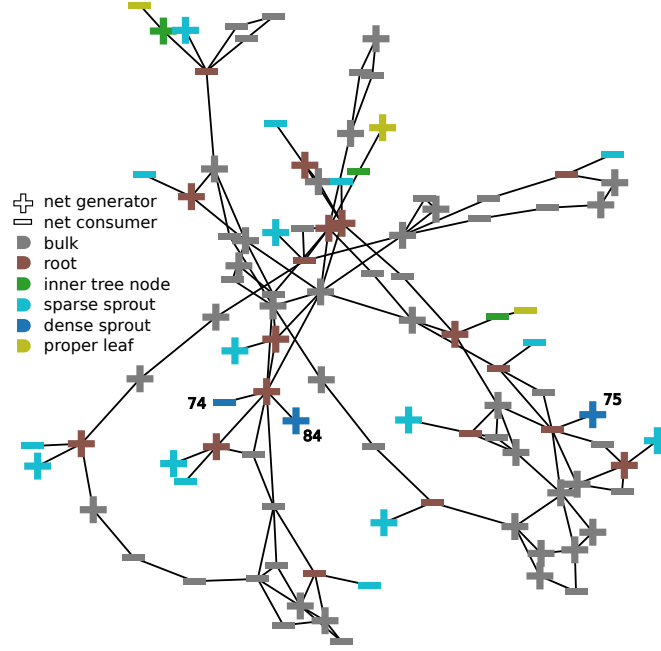


FIG. S2. A synthetic power grid of  $N = 100$  nodes and their topological classes according to reference [23]. Generated using a random growth model, see reference [33]. Nodes marked with a "+" ("−") have  $P_i = \pm 1$ . The grid and its three dense sprout nodes, highlighted with node numbers 74, 75 and 84, are used as examples throughout the figures of the main article and the supplement.

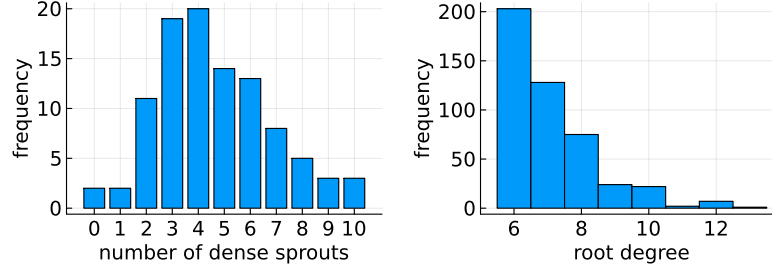


FIG. S3. Topological properties of the ensemble of 100 synthetic networks. (left) Histogram of the number of dense sprout nodes per network. (right) Histogram of the degrees of the respective root nodes. Each root node appears as many times as it has dense sprout nodes as neighbors.

modes, the solution can be shifted significantly from the network mode that is most localized at the root node, cf. Fig S6.

Fig. S7 shows a phase portrait of node 74 of grid 1, the grid in Fig. S2.

Fig. S8 compares the analytical prediction of the minimal effective model with simulation data from all 462 dense sprouts in the ensemble. Our prediction from the model reduction that the minimal model provides an upper bound are confirmed.

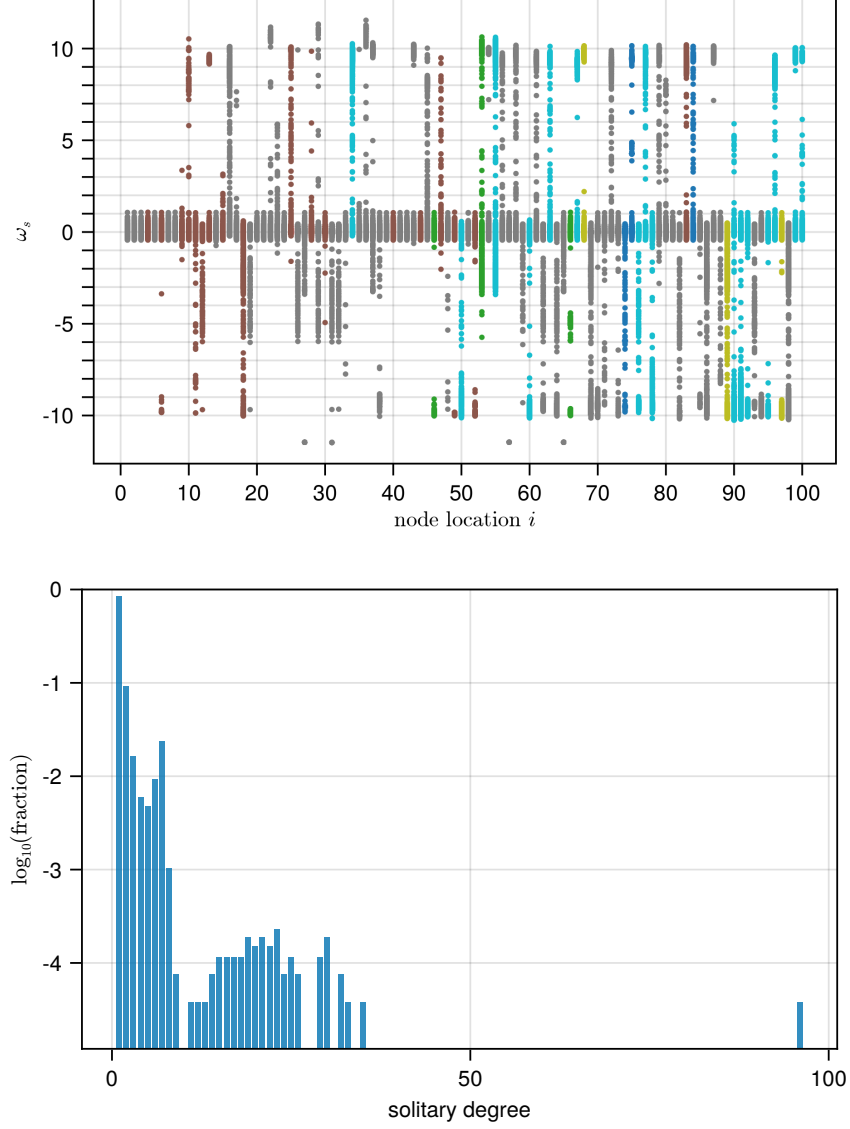


FIG. S4. Asymptotic frequencies in a synthetic power grid. We apply a fine mesh of 1,200 evenly spaced single-node perturbations to each of the 100 nodes in a synthetic power grid, see Fig. S2. About 22% of the perturbations lead to desynchronized asymptotic states. (top) The wide spectrum of possible asymptotic mean frequencies in this highly multistable system is scattered over the node locations. We see that the natural frequencies place approximate bounds on the asymptotic mean frequencies. The difference to Fig. 2 in the main article is that here, all asymptotic states are shown (not only 1-solitaires). (right) Histogram of the relative abundance of solitary degrees (numbers of desynchronized nodes, not degrees of solitary nodes) of all the desynchronized asymptotic states. In a single occasion, a single-node perturbation desynchronized the whole network.

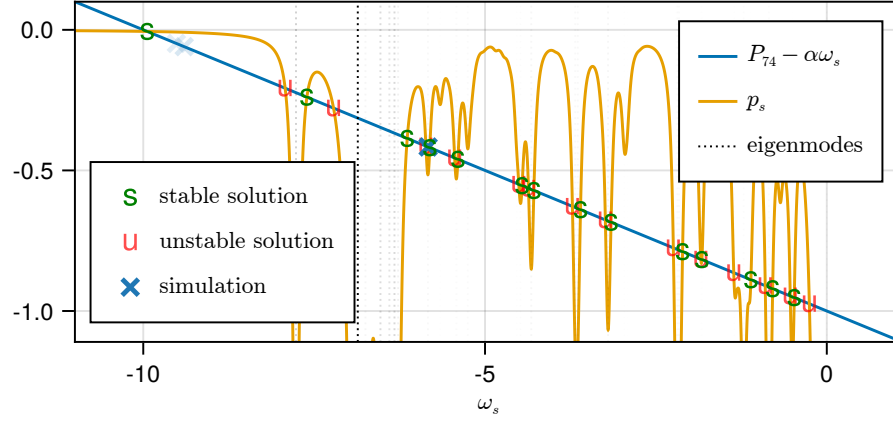


FIG. S5. Solutions of Eq. (S59) for a dense sprout node ( $i = 74$ ) in a synthetic power grid, see Fig. S2, with standard parameters. The number of intersections is much higher, but the simulations show qualitatively similar results.

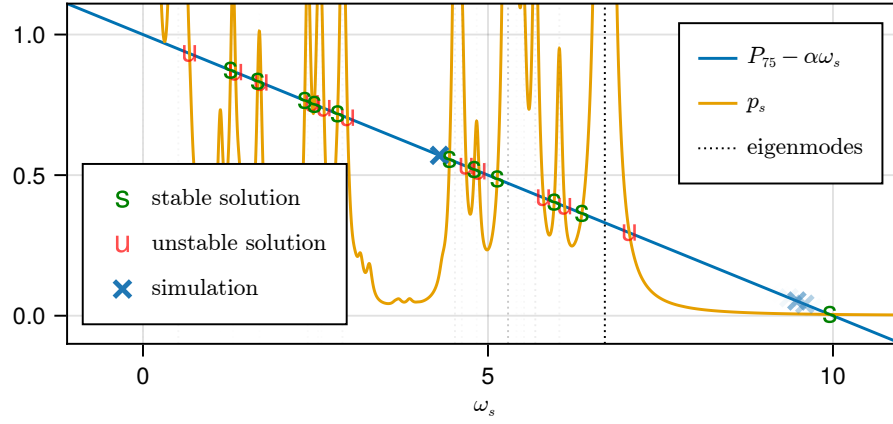


FIG. S6. Solutions of Eq. (S59) for a dense sprout node ( $i = 75$ ) in a synthetic power grid, see Fig. S2, with standard parameters. The landscape of network modes can shift the main solution far from the most localized network mode.

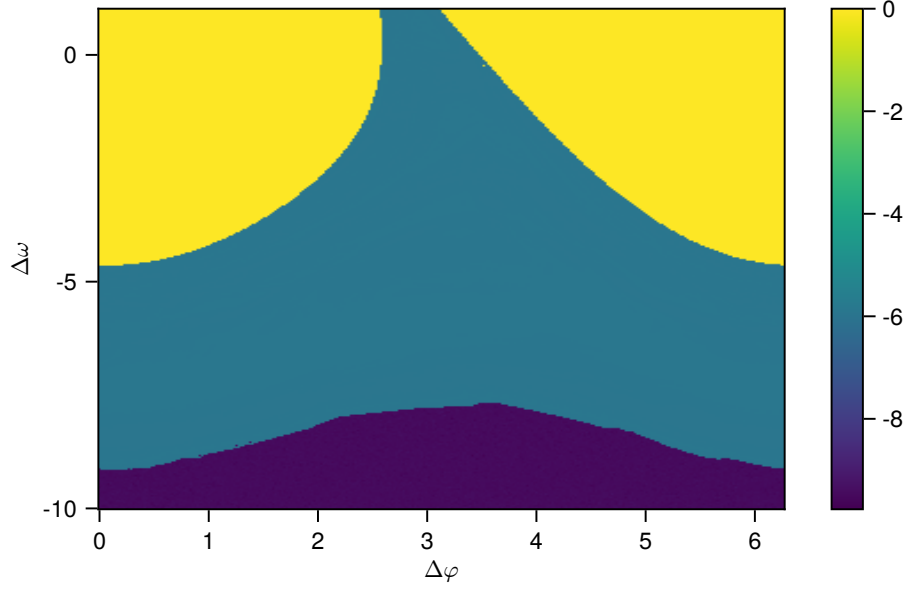


FIG. S7. Phase portrait of node 74 of grid 1. Color indicates the mean frequency after the transient following perturbations to the synchronous state with  $\Delta\varphi$  and  $\Delta\omega$  to  $\varphi_{74}$  and  $\omega_{74}$  respectively. Yellow is the synchronous state, turquoise a resonant solitary state, purple the natural solitary state.

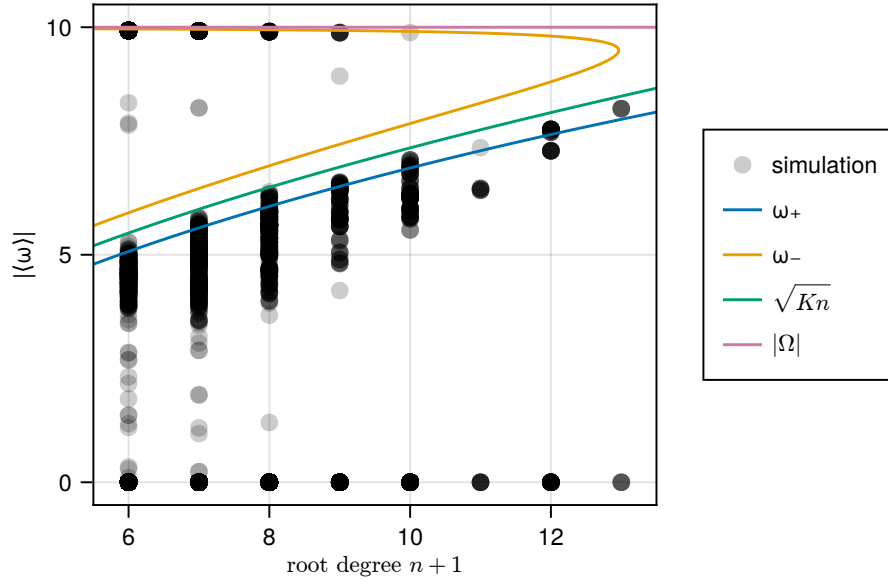


FIG. S8. The minimal effective model provides an upper bound for the mean frequencies of resonant solitary states, as seen by comparison with the simulation results from the ensemble of synthetic power grids. A mesh of single-node perturbations is applied to all dense sprout nodes in the ensemble. All asymptotic mean frequencies at the dense sprout nodes are then scattered and overlaid by the analytical solution for the effective toy model. The branches  $\omega_{\pm}$  correspond to  $\omega_s(n_{\pm})$  in Eq. (S84).  $\sqrt{Kn}$  is the network mode at the center between the branches.  $\Omega = \pm 10$  is the natural frequency of generators or consumers, respectively, and the asymptotic bound for the solitary frequencies.